Available online at www.sciencedirect.com
ScienceDirect
Journal of Photochemistry and Photobiology B: Biology 85 (2006) 1–16
Journal of Photochemistry and Photobiology B:Biology
www.elsevier.com/locate/jphotobiol

Absorption and fluorescence spectroscopic characterization of cryptochrome 3 from *Arabidopsis thaliana*

S.-H. Song [a], B. Dick [a], A. Penzkofer [b,*], R. Pokorny [c], A. Batschauer [c], L.-O. Essen [d]

[a] *Institut für Physikalische und Theoretische Chemie, Universität Regensburg, 93053 Regensburg, Germany*
[b] *Institut II – Experimentelle und Angewandte Physik, Universität Regensburg, Universitätstrasse 31, D-93053 Regensburg, Germany*
[c] *Fachbereich Biologie, Pflanzenphysiologie/Photobiologie, Philipps-Universität, Karl-von-Frisch-Strasse 8, D-35032 Marburg, Germany*
[d] *Fachbereich Chemie, Philipps-Universität Marburg, Hans-Meerwein-Strasse, D-35032 Marburg, Germany*

Received 8 October 2005; received in revised form 11 March 2006; accepted 22 March 2006
Available online 24 May 2006

Abstract

The blue light photoreceptor cryptochrome 3 (cry3) from *Arabidopsis thaliana* was characterized at room temperature in vitro in aqueous solution by optical absorption and emission spectroscopic studies. The protein non-covalently binds the chromophores flavin adenine dinucleotide (FAD) and *N*5,*N*10-methenyl-5,6,7,8-tetrahydrofolate (MTHF). In the dark-adapted state of cry3, the bound FAD is present in the oxidized form (FAD_{ox}, ca. 38.5%), in the semiquinone form ($FADH^{\cdot}$, ca. 5%), and in the fully reduced neutral form ($FAD_{red}H_2$) or fully reduced anionic form ($FAD_{red}H^-$, ca. 55%). Some amount of FAD (ca. 1.5%) in the oxidized state remains unbound probably caused by chromophore release and/or denaturation. Förster-type energy transfer from MTHF to FAD_{ox} is observed. Photo-excitation reversibly modifies the protein conformation causing a slight rise of the MTHF absorption strength and an increase of the MTHF fluorescence efficiency (efficient protein conformation photo-cycle). Additionally there occurs reversible reduction of bound FAD_{ox} to $FAD_{red}H_2$ (or $FAD_{red}H^-$, FAD_{ox} photo-cycle of moderate efficiency), reversible reduction of $FADH^{\cdot}$ to $FAD_{red}H_2$ (or $FAD_{red}H^-$, $FADH^{\cdot}$ photo-cycle of high efficiency), and modification of re-oxidable $FAD_{red}H_2$ (or $FAD_{red}H^-$) to permanent $FAD_{red}H_2$ (or $FAD_{red}H^-$) with low quantum efficiency. Photo-excitation of MTHF causes the reversible formation of a MTHF species (MTHF′, MTHF photo-cycle, moderate quantum efficiency) with slow recovery to the initial dark state, and also the formation of an irreversible photoproduct (MTHF″).

Keywords: Cryptochrome; *Arabidopsis thaliana*; Cry3; MTHF; FAD; Fluorescence spectroscopy; Absorption spectroscopy; MTHF–FAD interaction; Photo-reduction; Photo-cycle dynamics; Energy transfer

1. Introduction

Blue-light sensitive photoreceptors control many crucial biological processes (for reviews see [1,2]). Important blue-light receptor groups are (i) cryptochromes (Cry) [3–5] that are related to photolyases, and which regulate plant growth and development as well as the synchronization of the circadian rhythm in animals, (ii) BLUF domain receptors [6] for the control of photosynthetic gene expression (AppA from *Rhodobacter sphaeroides* [7]), for blue-light avoidance response (PAC from *Euglena gracilis* [8]), for probably positive phototaxis (Slr1694 from *Synechochocystis* sp. PCC6803 [9]), and for still unknown function (Tll0078 from *Thermosynechococcus elongates* BP-1 [10], BrlB from *Rhodobacter sphaeroides* [11,12]), and (iii) phototropins (phot) [13] for the regulation of phototropism and other movement responses in plants. The chromophores (cofactors) in photolyases are flavin-adenine-dinucleotide (FAD) together with either (*N*5,*N*10)-methenyl-5,6,7,8-tetrahydrofolate (MTHF) or 8-hydroxy-7,8-didemethyl-5-deaza-riboflavin (8-HDF), while in cryptochromes FAD and MTHF were identified as chromophores [14,15]. In

* Corresponding author. Tel.: +49 941 943 2107; fax: +49 941 943 2754.
E-mail address: alfons.penzkofer@physik.uni-regensburg.de (A. Penzkofer).

1011-1344/$ - see front matter © 2006 Elsevier B.V. All rights reserved.
doi:10.1016/j.jphotobiol.2006.03.007

the BLUF domain receptors the cofactor is FAD, and in the phototropins the chromophore is flavin-mono-nucleotide (FMN).

Cryptochromes are UV-A and blue-light photoreceptors in plants, animals, and bacteria with a high degree of sequence and structural homology to DNA photolyases but with no repair function [4]. In the plant *Arabidopsis thaliana* three cryptochromes, cry1 [16], cry2 [17], and cry3 [18] (the latter also called cry-DASH [19]) have been identified. Cry1 plays a major role in the de-etiolation response [20]. Cry2 is involved in the day-length perception for flower induction [21], whereas the biological function of cry3 is not yet known.

In this paper, we undertook an optical spectroscopic characterization of cry3 from *Arabidopsis thaliana*. Cry3 was studied in vitro in an aqueous buffer solution at room temperature. Some comparative studies on MTHF-Cl were carried out. The dark-state absorption and emission behaviour of cry3 was investigated, followed by analysis of the absorption and emission behaviour under light excitation in the visible and UV-A spectral range. The behaviour of the sample after light exposure in the dark was also analyzed. The specific effects due to the presence of two chromophores, FAD (non-covalently bound FAD_{ox}, $FADH^{\cdot}$, $FAD_{red}H_2$, small fraction of unbound FAD_{ox}) and MTHF, are elucidated. Structural formulae of these molecules are depicted in Fig. 1.

2. Experimental procedures

2.1. Sample preparation

Cloning, expression in *Escherichia coli* and chromatographic purification of cry3 has been described elsewhere [22]. In brief, cry3 was overexpressed in *E. coli* M15[pREP4] cells that were grown after IPTG (isopropyl-β-D-thiogalactoside) induction in 1.5 l of LB medium containing 100 μg ml^{-1} ampicillin and 25 μg ml^{-1} kanamycin at 30 °C for 12 h by shaking at 250 rpm. The overexpressed cry3 protein was then purified by the following chromatography steps on the ÄKTApurifier (Amersham Biosciences, Buckinghamshire, UK): By Ni^{2+}-affinity chromatography on a HisTrap HP column, by Heparin chromatography on HiTrap Heparin HP column, and finally by size-exclusion chromatography on Superdex 200 GL column in buffer containing 50 mM Na-phosphate pH 7.5, 200 mM NaCl, 10 mM β-mercaptoethanol and 10% glycerol. The final concentration of NaCl in the sample was adjusted to 50 mM, the other components remained unchanged (this final composition of the buffer is abbreviated as pH 7.5 buffer). Purified cry3 was concentrated to about 3–10 mg ml^{-1} as estimated by the Bradford method and analyzed by SDS–PAGE under reducing conditions. The identity of cry3 was confirmed by MALDI-TOF MS analysis (data not shown). The sample was divided into several aliquots, flash-frozen in liquid nitrogen and stored at −80 °C or

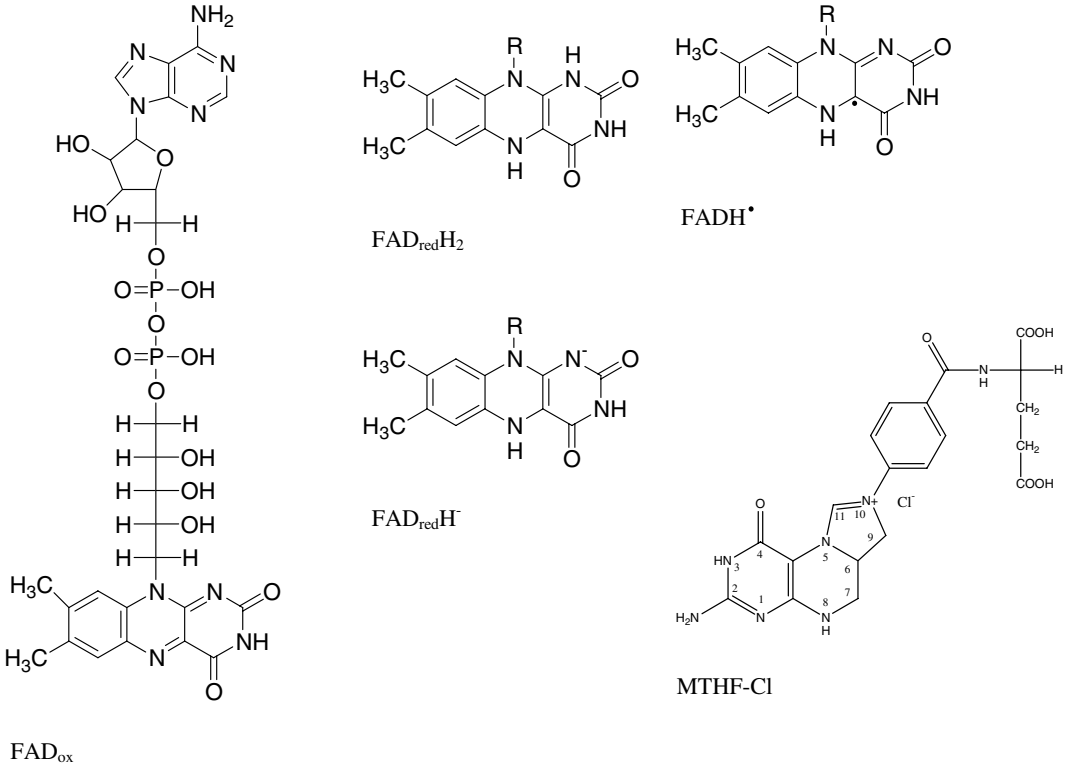

Fig. 1. Structural formulae of FAD in its oxidized form (FAD_{ox}), fully reduced neutral form ($FAD_{red}H_2$), fully reduced anionic form ($FAD_{red}H^-$), neutral semiquinone form ($FADH^{\cdot}$), and of MTHF-Cl.

−20 °C. The yield of purified protein was 2–3 mg per liter of induced *E. coli* culture. The cofactor composition and the ratio to cry3 apoprotein was determined after apoprotein precipitation with 7.2% (final, 440 mM) TCA (trichloroacetic acid) on ice for 1 h with shaking at 100 rpm followed by separation of the released cofactors by reversed phase chromatography on Nucleosil 100-10 C18 column connected to the ÄKTApurifier (Amersham Biosciences, Buckinghamshire, UK) and pre-equilibrated with a 9:1 mixture of phosphate–citrate buffer pH 2.5 (10 mM Na_2HPO_4 and 45 mM citric acid) and methanol. Upon releasing from the apoprotein, all different redox states of flavin should be converted to the oxidized form due to oxidation by air oxygen. Precipitated apoprotein was pelleted at 20,000*g* and 4 °C for 10 min, re-suspended in 1 M NaOH at 70 °C for 10 min, its absorption spectrum (not shown) was taken to ensure that it contains no remaining cofactors and its molar amount was estimated based on its absorbance, A_{280}, at 280 nm using the theoretical value of molar extinction coefficient at 280 nm for cry3 with no cystine (110,950 M^{-1} cm^{-1}) calculated by ProtParam software on ExPASy Proteomics server (www.expasy.org). Supernatant containing released cofactors was nine times diluted into the phosphate–citrate buffer pH 2.5 (final composition after dilution was as above) containing 49 mM NaOH (for neutralization of TCA), filtered through 0.2 μm filter (Sarstedt, Nümbrecht, Germany), mixed 9:1 with methanol and injected to the column. Cofactors were separated and eluted from the column using a continuous linear gradient of methanol (60–80%) mixed with the aforementioned buffer and monitored by absorption at 360 nm (both MTHF and oxidized flavin species) and 450 nm (only oxidized flavin species). For comparison, known amounts of each standard (MTHF-Cl, FAD, FMN and riboflavin) were processed analogously and aliquots corresponding to 5 nmols were separated as above. Based on the elution peak area ratios between cofactors released from cry3 and corresponding standards, a 1:1 MTHF to FAD ratio was found within the experimental accuracy while no other cofactor was present. The identities of released and separated cofactors were further confirmed by their absorption spectra which corresponded to those of standards (not shown). The ratio of cofactors to cryptochrome 3 protein was estimated to be 0.8:1 ($[FAD] = [MTHF] = 0.8 \times C_0$, where C_0 is the total cryptochrome 3 concentration) but could be higher due to some uncertainty in protein determination.

FAD was purchased by Sigma (flavin adenine dinucleotide disodium salt hydrate, order number F 6625) and was used without further purification. (6*R*,*S*)-5,10-methenyl-5,6,7,8-tetrahydrofolic acid chloride was purchased from Schircks Laboratories, CH-8646 Jona, Switzerland. It was used as delivered.

2.2. Spectroscopic techniques

Transmission measurements were carried out with commercial spectrophotometers. The absorption coefficient spectra, $\alpha(\lambda)$, and absorption cross-section spectra, $\sigma_a(\lambda)$, have been determined from the transmission spectra, $T(\lambda)$, by the relation, $T(\lambda) = \exp[-\alpha(\lambda)\ell] = \exp[-\sigma_a(\lambda)N_0\ell]$, where N_0 is the number density of molecules, and ℓ is the sample length.

The fluorescence spectra were measured with a self-assembled fluorimeter in front-face collection arrangement [23,24]. A mercury lamp together with appropriate interference filters were used as excitation source. The intrinsic fluorescence quantum distributions, $E_F(\lambda)$, were measured under conditions of vertical polarized excitation and magic-angle fluorescence detection (54.7°). A spectrometer – silicon-diode-array detection system was used for spectra recording (TN-1710 multichannel analyser with diode array rapid scan spectrometer system from Tracor Northern). For some fluorescence quantum distribution measurements on cry3 an intensified silicon-diode-array detector was used (OMA system from EG&G Princeton Applied Research) in order to lower the sample excitation necessary for fluorescence detection (avoidance of light-adapted state formation in fluorescence measurement process). The intrinsic fluorescence quantum yield, ϕ_F, is calculated by integration over the fluorescence quantum distribution [$\phi_F = \int E_F(\lambda)\, d\lambda$]. The dyes quinine-sulphate dihydrate in 1 N H_2SO_4 (fluorescence quantum yield, $\phi_{F,R}(C) = 0.546/(1 + 14.5C)$ where C is dye concentration in mol dm^{-3} [25], excitation wavelength $\lambda_{exc} = 365$ nm), and coumarin 314 T in ethanol ($\phi_{F,R} = 0.87$ according to technical data sheet of Kodak, $\lambda_{exc} = 428$ nm) were used as fluorescence standards. The degree of fluorescence polarization, $P_F = (S_{F,\parallel} - S_{F,\perp})/(S_{F,\parallel} + S_{F,\perp})$, was determined by measuring the fluorescence signal polarized parallel ($S_{F,\parallel}$) and perpendicular ($S_{F,\perp}$) to the excitation light.

Fluorescence lifetime measurements have been carried out with second harmonic light pulses of a mode-locked Ti:sapphire laser system (wavelength $\lambda_L = 400$ nm, duration $\Delta t_L \approx 3.5$ ps, laser system Hurricane from Spectra-Physics) together with a micro-channel-plate photomultiplier (type R1564-U01 from Hamamatsu) and a fast digital oscilloscope (LeCroy type DSO 9362, 710 ps FWHM of response function).

The dependence of the absorption coefficient spectra on the excitation intensity at fixed excitation wavelengths was studied by full illuminating a small-volume cell (size 1.5 mm × 1.5 mm × 5 mm) with a 200 W mercury lamp through interference filters. The excitation intensity was varied with neutral density filters. After a fixed period of mercury lamp light exposure, the transmitted white light of an attenuated tungsten lamp was recorded with the same spectrometer – diode-array detection system as used for the fluorescence measurements.

The photo-cycle behaviour at different excitation wavelengths was studied by recording transmission spectra during intense light exposure and in the dark after light exposure, and by measuring the spectral fluorescence development before, during and after light exposure.

Quantum efficiencies of protein and chromophore modification, ϕ_{mod}, are determined by measuring the fractions

of modified species, ΔN_{mod}, the fraction of absorbed photons by the considered species, $\Delta n_{\mathrm{ph,abs}}$, and calculating the ratio

$$\phi_{\mathrm{mod}} = \frac{\Delta N_{\mathrm{mod}}}{\Delta n_{\mathrm{ph,abs}}}. \quad (1)$$

3. Results

3.1. Absorption spectra

The absorption cross-section spectrum of dark-adapted cry3 in pH 7.5 buffer is shown by the solid curves in Fig. 2a, b, and the dotted curve in Fig. 2c. It was obtained from the transmission spectrum of a solution of concentration of $C_{\mathrm{w}} = 2$ mg/ml and a molar mass of $M_{\mathrm{w}} = 60{,}720$ g mol^{-1} (concentration $C = C_{\mathrm{w}}/M_{\mathrm{w}} = 3.3 \times 10^{-5}$ mol dm^{-3}). The other absorption cross-section spectra in Fig. 2b belong to FAD in aqueous solution at pH 7.0 (dashed line, FAD_{ox}, from [26]), to neutral reduced FAD ($FAD_{red}H_2$, triple-dotted curve, from [27]), to anionic reduced FAD ($FAD_{red}H^-$, dotted curve, from [27]), and neutral FAD semiquinone ($FADH^{\cdot}$, dash-triple-dotted curve, from [28]). In Fig. 2c, besides the cry3 spectrum, the absorption cross-section spectrum of MTHF released from *E. coli* photolyase (solid line, from [29]) and the absorption cross-section spectrum of MTHF-Cl in aqueous solution at pH 2.5 (aqueous HCl solution, dashed line) are shown.

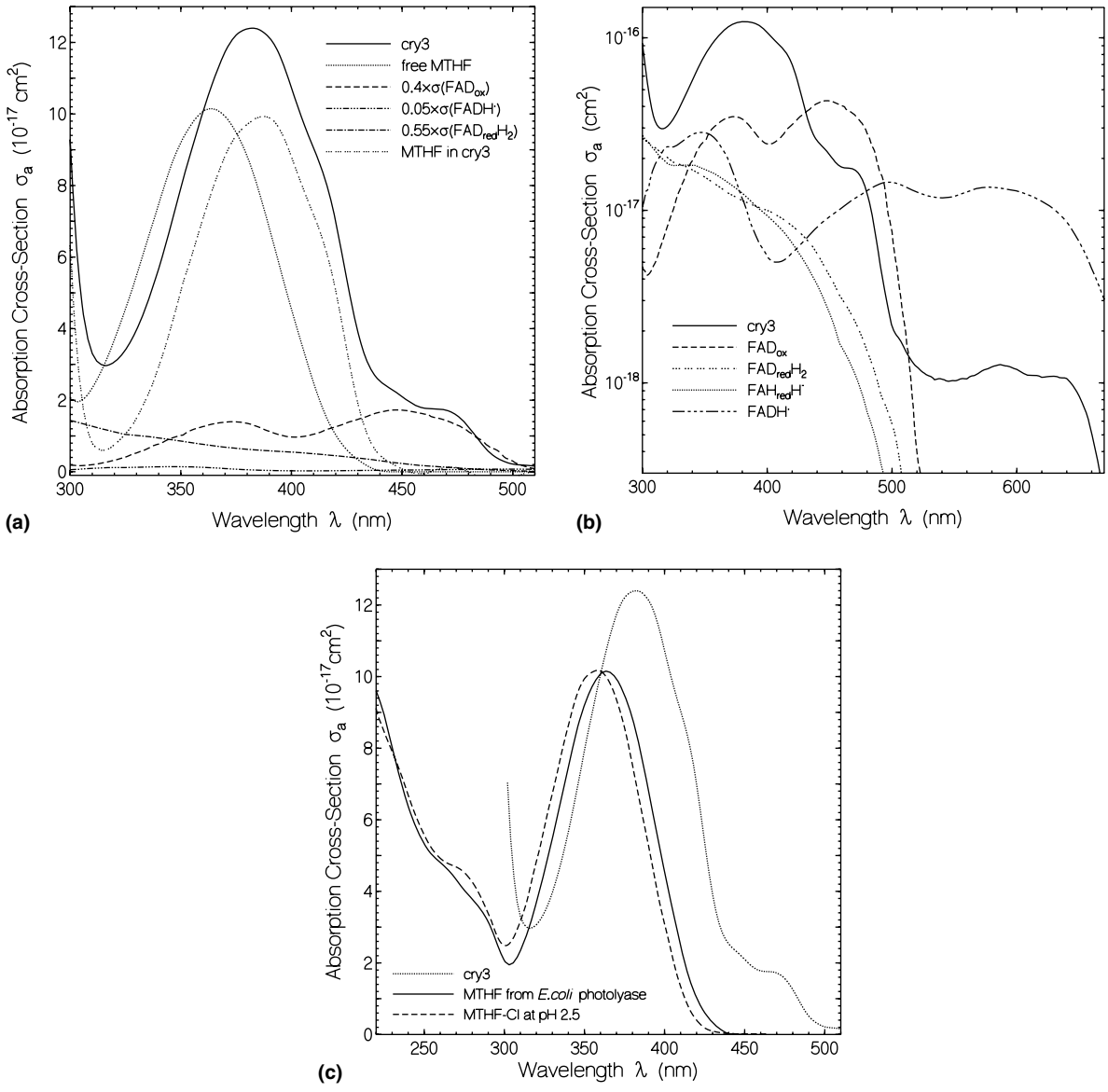

Fig. 2. (a) Absorption cross-section spectrum of dark-adapted cry3 (solid curve) together with absorption cross-section spectra of 40% FAD_{ox} in aqueous solution at pH 7.0, of 55% $FAD_{red}H_2$ in protein, of 5% FAD-semiquinone ($FADH^{\cdot}$), of released MTHF from *Escherichia coli* photolyase (dotted line), and residual spectrum, $\sigma_a(\mathrm{res}) = \sigma_a(\mathrm{cry3}) - 0.4 \times \sigma_a(FAD_{ox}) - 0.55 \times \sigma_a(FAD_{red}H_2) - 0.05 \times \sigma_a(FADH^{\cdot})$ (triple dotted line), thought to be due to MTHF in the protein. (b) Absorption cross-section spectra of cry3 in pH 7.5 buffer solution, FAD_{ox} in aqueous solution at pH 7.0, $FAD_{red}H_2$ (from [27]), $FAD_{red}H^-$ (from [27]), and $FADH^{\cdot}$ (from [28]). (c) Absorption cross-section spectra of cry3 in pH 7.5 buffer, MTHF released from *Escherichia coli* photolyase [29], and MTHF-Cl in aqueous solution at pH 2.5.

In Fig. 2a the dashed spectrum is given by $x_1\sigma_a(FAD_{ox})$, where $x_1 = 0.40$ is the expected mole-fraction of neutral oxidized FAD present in cry3 (96.3% thereof correctly bound and 3.7% thereof not fixed in the binding pocket probably caused by protein denaturation and chromophore release, see below). The dash-triple-dotted spectrum is given by $x_2\sigma_a(FADH^{\bullet})$, where $x_2 = 0.05$ is the mole-fraction of neutral FAD semiquinone. The dash-dotted curve is given by $x_3\sigma_a(FAD_{red}H_2)$, where $x_3 = 1 - x_1 - x_2 = 0.55$ is the expected mole-fraction of neutral reduced FAD in cry3 (anionic reduced FAD, $FAD_{red}H^-$, has a similar absorption spectrum and cannot be distinguished from $FAD_{red}H_2$ within our experimental accuracy). The triple-dotted line is the remaining difference, $\sigma_a(cry3) - x_1\sigma_a(FAD_{ox}) - x_2\sigma_a(FADH^{\bullet}) - x_3\sigma_a(FAD_{red}H_2)$. This remaining spectrum is thought to be the absorption cross-section spectrum of MTHF in cry3. For comparison the dotted line shows the absorption cross-section spectrum of free MTHF released from *Escherichia coli* photolyase [29] (see Fig. 2c). The spectral red-shift of MTHF in the protein is thought to be due to specific protein MTHF interaction [30,31].

3.2. Fluorescence studies

In Fig. 3 fluorescence quantum distributions, $E_F(\lambda)$, of cry3, FAD, and MTHF are shown. In part (a) the distributions are shown for dark-adapted cry3 in pH 7.5 buffer excited at 365 nm (dash-dotted curve, exposed energy density for fluorescence measurement $w_{exc} = 1 \times 10^{-4}$ J cm^{-2}, concentration 8 mg/ml) and at 450 nm (solid curve, corrected for edge filter absorption, $w_{exc} = 1 \times 10^{-4}$ J cm^{-2}), as well as for FAD in aqueous solution at pH 7.0 (taken from [26]) and for FAD in pH 7.5 buffer (excitation wavelength $\lambda_{exc} = 428$ nm). In the case of excitation at 450 nm the cry3 fluorescence belongs to FAD_{ox} excitation. The fluorescence quantum yield is rather small. A value of $\phi_F \approx 3 \times 10^{-3}$ is obtained. In the case of cry3 excitation at 365 nm about 10% of light is absorbed by FAD_{ox}, about 80% of light is absorbed by MTHF, and the rest is absorbed by $FAD_{red}H_2$ and $FADH^{\bullet}$. The fluorescence quantum efficiency is $\phi_F \approx 0.012$. It is dominated by MTHF emission. The peak at 520 nm comes from FAD_{ox} emission. It is larger than the expected emission from direct FAD_{ox} absorption. It is attributed to FAD_{ox} emission caused by MTHF to FAD_{ox} energy transfer. The fluorescence quantum yield of free FAD in pH 7.5 buffer with β-mercaptoethanol ($\phi_F \approx 0.07$) is a factor of two larger than that of FAD in neutral aqueous solution ($\phi_F \approx 0.033$) indicating some more un-stacked arrangement of the isoalloxazine and adenine moiety in pH 7.5 buffer with β-mercaptoethanol decreasing the efficiency of photo-induced electron transfer [26].

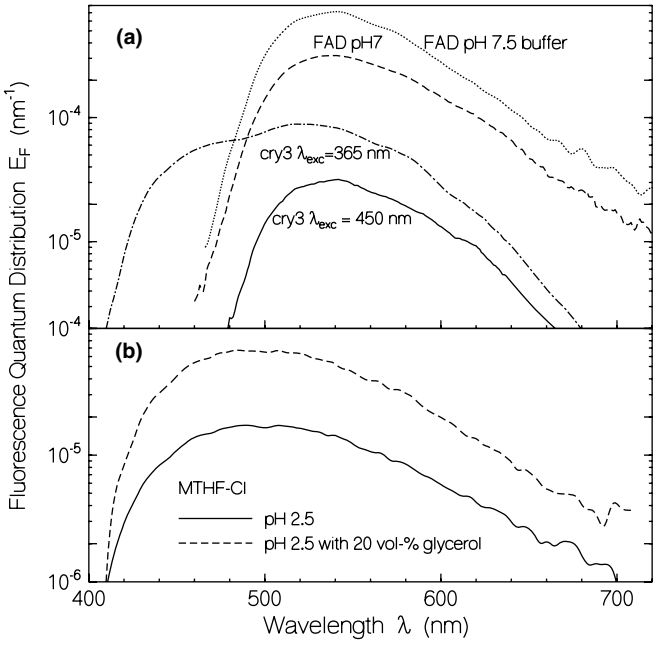

Fig. 3. (a) Fluorescence quantum distributions, $E_F(\lambda)$, of dark-adapted cry3 obtained for $\lambda_{exc} = 450$ nm (solid line) and 365 nm (dash-dotted line), FAD in pH 7.5 buffer (dotted line), and in aqueous solution at pH 7.0 (dashed line, from [8]). (b) Fluorescence quantum distributions, $E_F(\lambda)$, of MTHF-Cl in aqueous solution at pH 2.5, and in aqueous solution at pH 2.5 with 20 vol% glycerol.

In part (b) of Fig. 3 the fluorescence quantum distributions of MTHF-Cl in aqueous solution at pH 2.5, and in aqueous solution at pH 2.5 together with 20 vol% glycerol are shown. The samples were excited at $\lambda_{exc} = 365$ nm. The fluorescence quantum yield of MTHF-Cl in aqueous solution at pH 2.5 is $\phi_F \approx 2.5 \times 10^{-3}$. Addition of 20-vol% glycerol (increase in viscosity) increased the fluorescence quantum yield to $\phi_F \approx 9.2 \times 10^{-3}$. It is thought that the efficiency of internal conversion is reduced by the increase in viscosity.

The polarization dependence of the fluorescence spectra is shown in Fig. 4. In parts (a, b, c) fluorescence spectra are shown for parallel polarized ($S_{F,\parallel}$) and perpendicular polarized ($S_{F,\perp}$) fluorescence light relative to the linear vertical polarization of the excitation light. In the parts (d, e, f) the corresponding degrees of fluorescence polarization, $P_F = (S_{F,\parallel} - S_{F,\perp})/(S_{F,\parallel} + S_{F,\perp})$ are shown. The curves shown in Fig. 4a and d belong to cry3 in pH 7.5 buffer with excitation at 365 nm. For $\lambda < 470$ nm the degree of fluorescence polarization is large. This fluorescence results from MTHF emission. There occurs no molecular reorientation within the fluorescence lifetime. For $\lambda > 470$ nm the degree of fluorescence-polarization decreased. The excitation energy transfer from MTHF to FAD_{ox} reduced the parallel orientation between the absorption and emission transition dipole moment. The energy transfer is most clearly seen for the perpendicular component since in the case of reorientation the perpendicular fluorescence signal gets larger. For the parallel polarized component the opposite is the case.

In Fig. 4b and e the polarization dependent fluorescence of cry3 in pH 7.5 buffer for $\lambda_{exc} = 450$ nm is shown (500 nm long-pass edge filter is in). The fluorescence belongs to FAD_{ox} emission. The degree of fluorescence polarization is wavelength independent and small. This indicates that

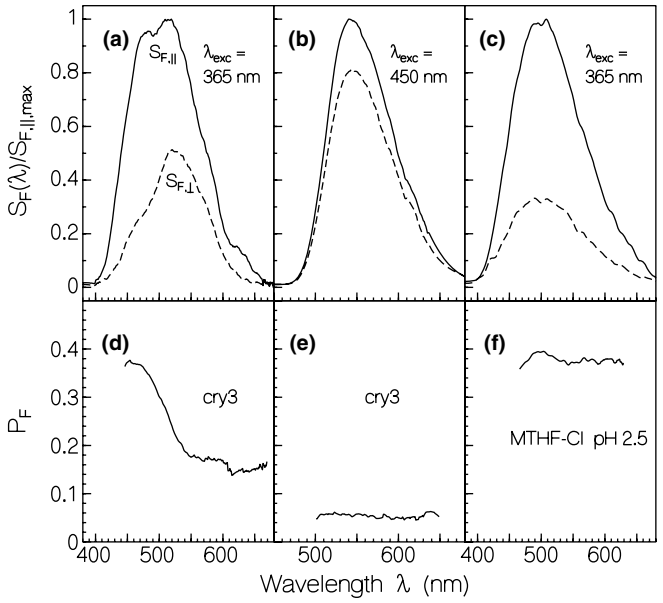

Fig. 4. Polarized fluorescence spectra, $S_{F,\|}(\lambda)$, $S_{F,\perp}(\lambda)$, and degrees of fluorescence polarization, $P_F(\lambda)$. (a) and (d) dark-adapted cry3 in pH 7.5 buffer. $\lambda_{exc} = 365$ nm, concentration 8 mg/ml. (b) and (e) dark-adapted cry3 in pH 7.5 buffer. $\lambda_{exc} = 450$ nm, concentration 8 mg/ml. (c) and (f) MTHF-Cl in aqueous solution at pH 2.5. $\lambda_{exc} = 365$ nm, concentration 2.3×10^{-4} mol dm^{-3}.

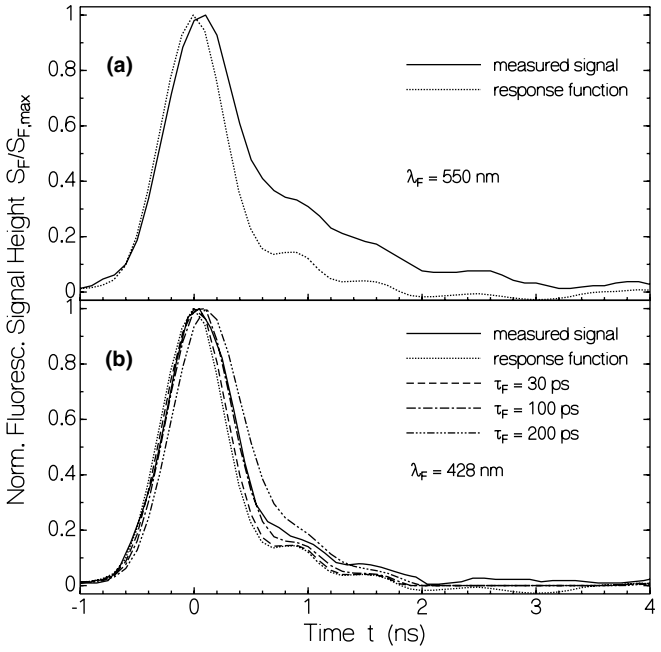

Fig. 5. Temporal fluorescence signals of dark-adapted cry3 sample (solid lines). Small-signal transmission $T_0 = 0.952$. Excitation at 400 nm with pulses of 3.5 ps duration. The signal was detected with a micro-channel-plate photomultiplier. Dotted lines show response function. (a) Detection at 550 nm (MTHF and FAD emission). (b) Detection at 428 nm (MTHF emission). Three convolution fits are included (Eqs. (2) and (3)). Fit parameter, τ_F, given in figure. Best fit $\tau_F = 100$ ps.

the fluorescence signal is dominated by the fraction of not properly fixed FAD_{ox} with rather long fluorescence lifetime since the fluorescence lifetime of FAD_{ox} in the protein is very short (U-shaped conformation causing photo-induced electron-transfer between isoalloxazine and adenine moiety).

In Fig. 4c and f the fluorescence polarization situation is shown for MTHF-Cl in aqueous solution at pH 2.5 for $\lambda_{exc} = 365$ nm. The degree of fluorescence polarization is rather high and wavelength independent. The fluorescence quantum yield is very low ($\phi_F \approx 0.0048$) resulting in a very short fluorescence lifetime. Within this short lifetime the excited molecules do not get reoriented.

Temporal fluorescence signal traces are shown in Fig. 5 (solid curves, excitation at 400 nm). The solid trace in Fig. 5a belongs to a fresh sample with fluorescence collection at 550 nm where MTHF and FAD_{ox} emit. The presented trace in Fig. 5b also belongs to a fresh cry3 sample, but with fluorescence collection at 428 nm (MTHF emission). The response function, $g(t)$, of the detection system is included in the figures by the dotted lines (FWHM-duration $\Delta t_{res} = 710$ ps, $1/e$-time constant $t_{res} = 460$ ps). It was determined by direct detection of the excitation picosecond laser pulse after strong attenuation.

To determine the fluorescence lifetime of MTHF in cry3 from the experimental trace in Fig. 5b, convolution curves were calculated using the experimental response function according to [26]

$$S_{F,con}(t) = \int_{-\infty}^{t} g(t') S_{F,\delta}(t - t')\, dt', \tag{2}$$

and a single-component, single-exponential excitation decay

$$S_{F,\delta}(t) = S_0 \exp(-t/\tau_F), \tag{3}$$

is used. A good agreement with the experimental data is obtained for $\tau_F(\text{MTHF}) = 100 \pm 50$ ps.

The fluorescence trace in Fig. 5a ($\lambda_{exc} = 400$ nm, $\lambda_F = 550$ nm) is composed of MTHF emission and FAD_{ox} emission. It indicates a fast and a slow relaxation. A regression fit of the slowly relaxing tail gives a lifetime of $\tau_{F,sl} \approx 1.1$ ns. It is attributed to non-correctly fixed FAD_{ox} or free FAD_{ox}. If we assume that the fluorescence emission in the case of 450 nm excitation is nearly completely due to not correctly bound (free) FAD_{ox}, then the fraction of free FAD_{ox} to total FAD_{ox} is estimated to be $\beta_{free} \approx \phi_F$(cry3,450 nm)/$\phi_F$($FAD_{ox}$ in pH 7.5 buffer) ≈ 0.037 (this is 1.5% of total FAD amount since the mole-fraction of oxidized FAD is 40%). Without free FAD_{ox} a fluorescence lifetime of the non-covalently bound FAD_{ox} of $\tau_F = \phi_F \tau_{rad} \approx 59$ ps would be estimated ($\phi_F = 0.003$, $\tau_{rad} = 19.5$ ns [32] is radiative lifetime of FAD_{ox}), but because of the presence of free FAD_{ox} it has to be considerably less.

3.3. Thermal stability

The room-temperature thermal stability of the samples was studied by measuring transmission spectra at certain time intervals after sample thawing. For this purpose the

sample was thermostated to $\vartheta = 20$ °C. The absorption spectra kept unchanged up to 6 h, then spectral changes due to light scattering appeared indicating continued protein aggregation and denaturation. Severe scattering occurred after 12 h. At $\vartheta = 26$ °C spectral changes due to light scattering (protein unfolding) started already after 15 min and became severe after 2 h.

3.4. Photo-cycle dynamics and photo-degradation dynamics

Changes of the absorption spectra of cry3 due to light exposure at different excitation wavelengths are shown in Fig. 6. The samples were exposed for durations of $t_{exp} = 20$ min with different excitation intensities, I_{exc}. The transmission was probed with an attenuated tungsten lamp. In the case of long-wavelength excitation ($\lambda_{exc} = 470$ nm, Fig. 6a, only FAD excitation) the absorption in the 440–490 nm region decreased. We think that FAD in the oxidized form (FAD_{ox}) changes to the fully reduced neutral form ($FAD_{red}H_2$) or to the fully reduced anionic form ($FAD_{red}H^-$) by photo-excitation. Excitation at 428 nm (Fig. 6b, FAD and MTHF excitation) again decreased the absorption in the FAD_{ox} region and caused some absorption decrease in the MTHF transition region. Excitation at 407 nm (Fig. 6c) and 365 nm (Fig. 6d) caused a stronger decrease of the MTHF absorption band than excitation at 428 nm (MTHF absorption dominates over FAD_{ox} absorption).

The change of the length-averaged absorption coefficient, $\bar{\alpha}(\lambda_{pr}) = -\ln[T(\lambda_{pr})]/\ell$, versus excitation intensity (20 min exposure) is shown in Fig. 7a for the probe wavelength $\lambda_{pr} = 473$ nm (change of FAD_{ox} content) and in Fig. 7b for $\lambda_{pr} = 386$ nm (dominant change of MTHF content). The dependencies are shown for the excitation wavelengths $\lambda_{exc} = 470$, 428, 407, and 365 nm.

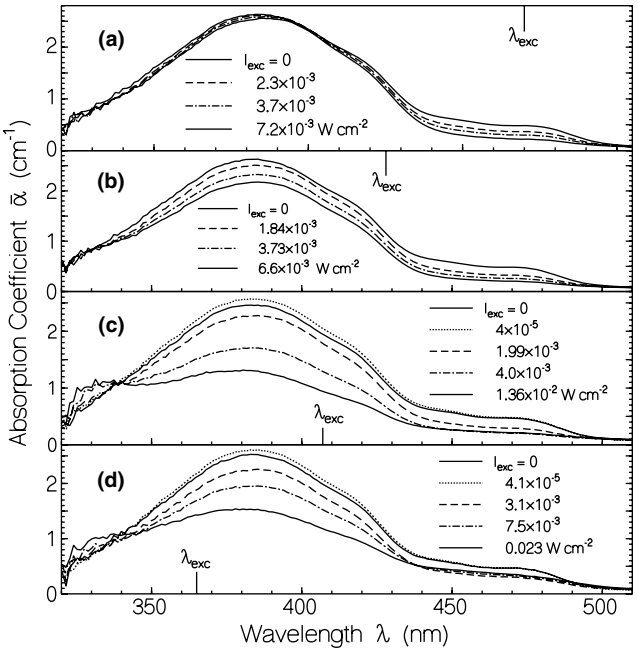

Fig. 6. Change of absorption spectra due to light exposure at different wavelengths and different excitation intensities. In all cases, spectra were recorded after 20 min of exposure. For excitation intensities $I_{exc} \geqslant 10^{-3}$ W cm^{-2} each time a fresh sample was used. (a) $\lambda_{exc} = 470$ nm, (b) $\lambda_{exc} = 428$ nm, (c) $\lambda_{exc} = 407$ nm, (d) $\lambda_{exc} = 365$ nm.

In Fig. 7a (FAD_{ox} absorption) and more pronounced in Fig. 7b (dominant MTHF absorption) a slight increase of absorption is seen in the intensity range from $I_{exc} \approx 10^{-6}$–10^{-4} W cm^{-2}. This is seen in more detail in the insets for $\lambda_{exc} = 428$ nm belonging to a sample of lower initial absorption coefficient. The slight increases of absorption seem to be caused by photo-induced structural

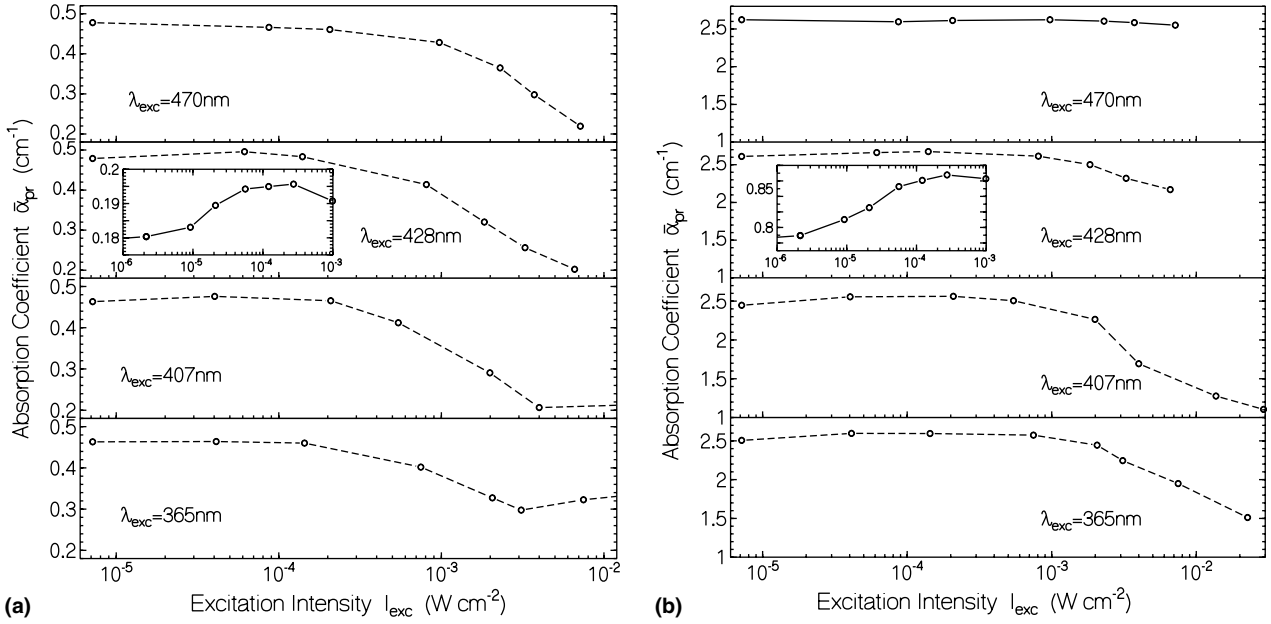

Fig. 7. Intensity dependent reduction of absorption coefficient of cry3 at (a) $\lambda_{pr} = 473$ nm and (b) $\lambda_{pr} = 386$ nm. For each data point the exposure time was 20 min. The excitation wavelengths, λ_{exc}, are given in the sub-pictures. Inserts show details (sample concentration: 0.75 mg/ml).

protein changes (non-radiative deactivation energy used to structurally change the surrounding protein, change of angular structure of chromophores, change of Franck–Condon overlap integrals). At high excitation intensities the absorption at $\lambda_{pr} = 473$ nm (Fig. 7a, FAD_{ox} absorption) and at $\lambda_{pr} = 386$ nm (Fig. 7b, dominant MTHF absorption) decreases. Application of even higher excitation intensities than displayed (20 min exposure-time) led to enhanced light scattering (protein unfolding).

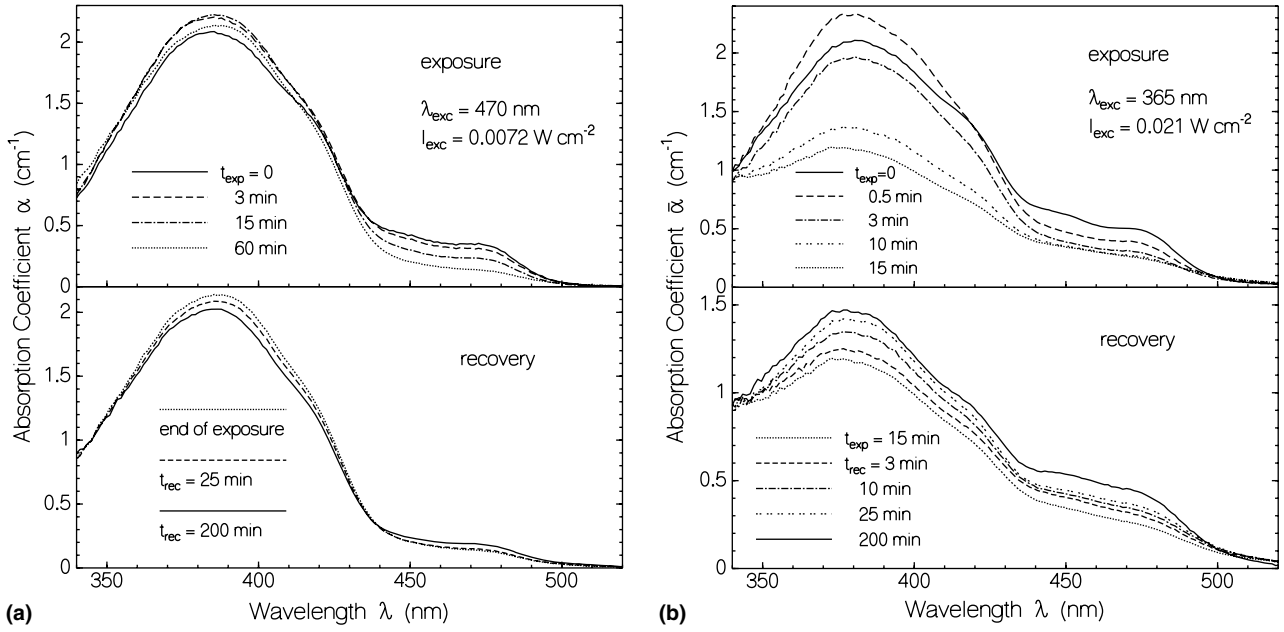

Fig. 8. Spectral photo-cycle behaviour of cry3 in pH 7.5 buffer. (a) Top part: Absorption change due to excitation. Excitation wavelength, $\lambda_{exc} = 470$ nm; excitation intensity, $I_{exc} = 0.0072$ W cm^{-2}. The exposure times, t_{exp}, are given in the figure. Lower part: Absorption recovery in the dark after 1 h of exposure. The times in darkness, t_{rec}, are given in the figure. (b) Top part: Absorption change due to excitation at $\lambda_{exc} = 365$ nm with $I_{exc} = 0.021$ W cm^{-2}. Lower part: Absorption recovery in the dark after 15 min of exposure.

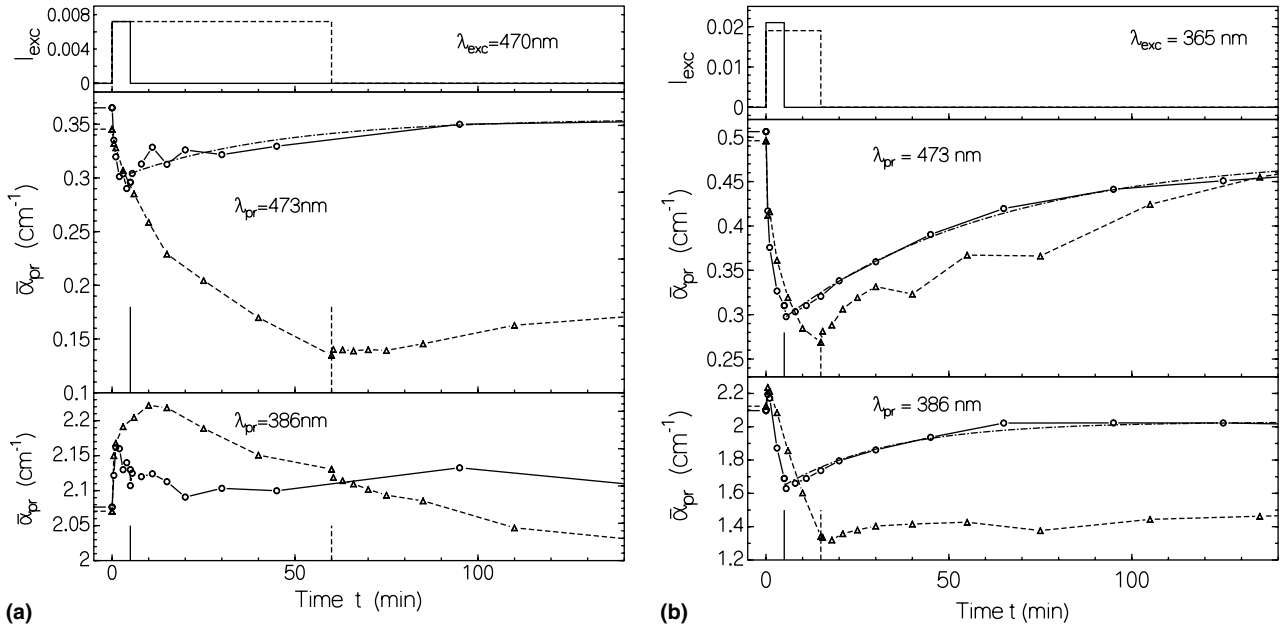

Fig. 9. Temporal photo-cycle behaviour of cry3 in pH 7.5 buffer. (a) Excitation at $\lambda_{exc} = 470$ nm for 5 min or 60 min and probing at $\lambda_{pr} = 473$ nm (peak absorption of FAD_{ox}) and $\lambda_{pr} = 386$ nm (peak absorption of MTHF in cry3). Solid lines belong to 5 min exposure; dashed lines belong to 60 min exposure. Dash-dotted curve in middle part is calculated for $\tau_{rec} = 42$ min (Eq. (4)). (b) Excitation at $\lambda_{exc} = 365$ nm for 5 min or 15 min and probing at $\lambda_{pr} = 473$ nm and $\lambda_{pr} = 386$ nm. Solid lines belong to 5 min exposure; dashed lines belong to 15 min exposure. Dash-dotted curves are calculated for $\tau_{rec} = 58$ min (middle part) and 30 min (lower part).

In Figs. 8 (spectral changes at certain times) and 9 (temporal development at two probe wavelengths) the photocycle dynamics of cry3 is presented. In the upper part of Fig. 8a the sample was excited at $\lambda_{exc} = 470$ nm where only FAD_{ox} is absorbing. During exposure the S_0–S_1 absorption of FAD_{ox} decreases and the absorption in the dominant S_0–S_1 absorption region of MTHF first increases and then decreases. We think that some photo-induced conversion of FAD_{ox} to $FAD_{red}H_2$ or $FAD_{red}H^-$ occurs. Conformational changes in the protein environment may be responsible for the slightly increased MTHF absorption. In the lower part of Fig. 8a the spectral change of absorption in the dark after 60 min of light exposure at $I_{exc} = 0.0072$ W cm^{-2} is displayed. The S_0–S_1 absorption of FAD_{ox} increases only slightly, the original absorption strength is not reached. Therefore, some amount of the photochemically reduced FAD seems to be resistant against oxidation under the experimental conditions. If the sample is only exposed for 5 min (spectra are not shown), then a nearly complete dark recovery to the FAD_{ox} absorption is observed (conversion of $FAD_{red}H_2$ and/or $FAD_{red}H^-$ back to FAD_{ox}). The dynamics described for 470 nm excitation is shown in Fig. 9a for two photo-cycles with different times of exposure (top part of Fig. 9a). The development of the absorption coefficients at the probe wavelengths, $\lambda_{pr} = 473$ nm (long-wavelength S_0–S_1 absorption peak of FAD_{ox}, middle part) and $\lambda_{pr} = 386$ nm (S_0–S_1 absorption peak of MTHF, lower part) is shown.

In the middle part of Fig. 9a the absorption recovery at $\lambda_p = 473$ nm after short-time exposure at $\lambda_{exc} = 470$ nm is fitted by the single-exponential function

$$\alpha_{pr}(t) = (\alpha_{pr,\infty} - \alpha_{pr,e})\{1 - \exp[-(t - t_e)/\tau_{rec}]\} + \alpha_{pr,e} \qquad (4)$$

where $\alpha_{pr,\infty}$ is the final absorption coefficient after long time of recovery, and $\alpha_{pr,e}$ is the absorption coefficient at the end of light exposure at time t_e. An approximate recovery time of $\tau_{rec} \approx 42$ min is obtained. The absorption difference, $\alpha_{pr}(0) - \alpha_{pr}(\infty)$, is likely due to permanent $FAD_{red}H_2$ or $FAD_{red}H^-$ formation.

Application of Eq. (1) to the initial absorption decrease in the middle part of Fig. 9a gives a quantum efficiency of FAD_{ox} reduction of $\phi_{FAD,red} \approx 0.0018$, where $\Delta N_{mod} = \Delta N_{FAD_{ox}}\ell = x_1 N_0 \ell[\alpha_{pr}(t_{exp}) - \alpha_{pr}(0)]/\alpha_{pr}(0)$ and $\Delta n_{ph,abs} = I_{exc} t_{exp}\{1 - [T_{pr}(0) + T_{pr}(t_{exp})]/2\}/(h\nu_{exc})$ has been used.

N_0 is the initial number density of cry3 molecules, x_1 is the mole-fraction of FAD_{ox}, and ℓ is the sample length.

The quantum efficiency, $\phi_{FAD,red,per}$, of permanent reduced FAD formation may be estimated from the incomplete absorption recovery after photo-excitation as seen in the middle part of Fig. 9a. Application of Eq. (1) with $\Delta N_{mod} = \Delta N_{FAD_{red,per}}\ell = x_1 N_0 \ell[\alpha_{pr,\infty} - \alpha_{pr}(0)]/\alpha_{pr}(0)$ and $\Delta n_{ph,abs} = I_{exc} t_e\{1 - [T_{pr}(0) + T_{pr}(t_e)]/2\}/(h\nu_{exc})$, with t_e the total exposure time, gives a value of $\phi_{FAD,red,per} \approx 4.3 \times 10^{-4}$.

In the lower part of Fig. 9a the absorption development at 386 nm (peak position of MTHF absorption) is shown. During light exposure the absorption first rises steeply, towards a maximum and then decreases slowly. At light switch-off there is an indication of a small fast absorption decrease followed by slow absorption change or nearly constant absorption. The initial absorption rise is thought to be due to MTHF absorption modification by some structure change of the surrounding protein. The quantum efficiency of absorption rise by protein modification (MTHF absorption rise), $\phi_{a,rise,MTHF}$, is, according to Eq. (1), given by the length-integrated number density of modified MTHF molecules, $\Delta N_{mod} = \Delta N_{MTHF}\ell = N_0\ell[\alpha_{pr}(t_{exp}) - \alpha_{pr}(0)]/[\alpha_{pr,max} - \alpha_{pr}(0)]$, to the number density of absorbed photons, $n_{ph,abs} = [1 - \overline{T}(\lambda_{exc})]\ t_{exp} I_{exc}/(h\nu_{exc})$, where $\overline{T} = [T(t_{exp}) + T(0)]/2$. Using the parameters of Fig. 9a ($t_{exp} = 30$ s, $\alpha_{pr}(t_{exp}) - \alpha_{pr}(0) = 0.0796$ cm^{-1}, $\alpha_{pr,max} - \alpha_{pr}(0) = 0.151$ cm^{-1}, $I_{exc} = 0.0072$ W cm^{-2}, $\lambda_{exc} = 470$ nm, $\overline{T}(\lambda_{exc}) = 0.95$) we find $\phi_{a,rise,MTHF} = 0.1$. The light absorption of FAD causes an absorption change of reversible MTHF with a quantum efficiency of about 10% by signalling via protein information transfer. The low-intensity absorption rise at $\lambda_{pr} = 473$ nm shown in the inset of Fig. 7a gives a similar efficiency, $\phi_{a,rise,FAD}$, of FAD_{ox} absorption change.

The decrease of the MTHF absorption band at prolonged light exposure is due to reversible MTHF conversion (most likely by changes in the MTHF binding site) and irreversible MTHF degradation (likely release of MTHF from the protein followed by hydrolysis to 5-formyltetrahydrofolate [33] or 10-formyltetrafolate [45]). The small sharp steps after light switch-off in the lower (386 nm) and middle part (473 nm) of Fig. 9a seem to indicate a partial fast back recovery to the original situation.

In the upper part of Fig. 8b the sample was excited at $\lambda_{exc} = 365$ nm where MTHF and FAD_{ox} are absorbing. During exposure, the S_0–S_1 absorption of FAD_{ox} decreases and the absorption in the dominant S_0–S_1 absorption region of MTHF first increases and then decreases. We think that the initial MTHF absorption increase is caused by photo-induced protein re-structuring as described above. The following absorption reduction in the MTHF absorption region is thought to be caused by a reversible modification of MTHF to MTHF′ and an irreversible modification to MTHF″ probably by cofactor release from the protein followed by hydrolysis together with FAD_{OX} reduction. In the lower part of Fig. 8b the spectral change of absorption in the dark after 15 min of light exposure at $I_{exc} = 0.021$ W cm^{-2} is displayed. The S_0–S_1 absorption of FAD_{ox} recovers nearly fully, while the MTHF absorption recovers only partly. MTHF′ recovers back to MTHF (MTHF photo-cycle), while MTHF″ is a permanent photoproduct (MTHF photo-degradation). If the sample is only exposed for 5 min, a nearly complete absorption spectrum recovery is observed (spectra are not shown, see temporal behaviour in lower part of Fig. 9b). It should be noticed that for longer exposure at 365 nm ($t_{exp} > 15$ min) the protein became denatured, which was reflected in a strong increase in light scattering.

The described dynamics for the 365 nm excitation is shown in Fig. 9b for two photo-cycles with different times of exposure (top part of Fig. 9b). The development of the absorption coefficients at the probe wavelengths, $\lambda_{pr} = 473$ nm (long-wavelength S_0–S_1 absorption-peak of FAD_{ox}, middle part) and $\lambda_{pr} = 386$ nm (S_0–S_1 absorption-peak of MTHF, lower part) is shown. In the middle part of Fig. 9b the absorption recovery at $\lambda_p = 473$ nm after short-time exposure at $\lambda_{exc} = 365$ nm is fitted by Eq. (4) An approximate recovery time of $\tau_{rec,FAD} \approx 58$ min is obtained. A similar fit in the lower part of Fig. 9b gives a recovery time of MTHF′ to MTHF of $\tau_{rec,MTHF} \approx 30$ min. Application of Eq. (1) to the early absorption decrease in the lower part of Fig. 9b gives a quantum efficiency of MTHF conversion to MTHF′ of $\phi_{MTHF'} \approx 2.9 \times 10^{-4}$ ($\Delta N_{mod} = \Delta N_{MTHF}\ell = N_0\ell\Delta\alpha_{pr}/\alpha_{pr}(0)$, $\Delta n_{ph,abs} = \delta t_{exp} I_{exc}[1 - \overline{T}(\lambda_{exc})]/(h\nu_{exc})$, δt_{exp} is the considered exposure interval, $\overline{T}(\lambda_{exc})$ is the average transmission at the excitation wavelength during exposure interval). The not complete absorption recovery after photo-excitation leads to a quantum efficiency of MTHF″ formation of $\phi_{MTHF''} \approx 3.7 \times 10^{-5}$($\Delta N_{mod} = \Delta N_{MTHF''}\ell = N_0\ell[\alpha_{pr,\infty} - \alpha_{pr}(0)]/\alpha_{pr}(0)$, and $\Delta n_{ph,abs} = t_e I_{exc}\{1 - [T(\lambda_{exc},0) + T(\lambda_{exc},t_e)]/2\}/(h\nu_{exc})$).

In cry3 approximately $x_2 \approx 5\%$ of the flavin adenine dinucleotide is in the semiquinone state (FADH·, see Fig. 2). The light exposure dependent absorption behaviour of FADH· in cry3 is shown in Fig. 10. A highly concentrated sample was used in the experiments ($C_w =$ 85 mg/ml corresponding to $C = 1.4 \times 10^{-3}$ mol dm^{-3}). The sample was excited at $\lambda_{exc} = 589$ nm with an intensity of $I_{exc} = 2.54 \times 10^{-3}$ W cm^{-2}. Absorption spectra measured at different times of exposure are shown in Fig. 10a. The FADH· absorption decreased with exposure time. The FADH· absorption recovery in the dark is shown in Fig. 10b. The absorption practically fully recovered with a time constant of about 60 min. The quantum efficiency, $\phi_{sq,red}$, of FAD-semiquinone reduction to FAD-hydroquinone may be calculated by application of Eq. (1) to the experimental situation [($\Delta N_{mod} = \Delta N_{FADH\cdot}\ell = x_2 N_0\ell[\alpha_{pr}(0) - \alpha_{pr}(t_{exp})]/\alpha_{pr}(0)$), and $\Delta n_{ph,abs} = t_{exp} I_{exc}[1 - \overline{T}(\lambda_{exc})]/(h\nu_{exc})$]. A value of $\phi_{sq,red} \approx 0.07$ is extracted from the data in Fig. 10.

The temporal absorption behaviour of FADH· in the case of excitation of FAD_{ox} in cry3 (≈ 8.5 mg/ml) at $\lambda_{exc} = 470$ nm is displayed in Fig. 11. During excitation the FADH· absorption decreases (Fig. 11a) as in the case of the long-wavelength excitation of FADH·. No photo-induced transfer from excited FAD_{ox} to FADH· is observed. This indicates that the FAD_{ox} reduction to $FAD_{red}H_2$ or $FAD_{red}H^-$ does not proceed via FADH· formation. Reduction of photo-excited FAD_{ox} (FAD^*_{ox}) to $FAD_{red}H_2$ via excited FADH· (FADH·*) might occur according to

$$FAD_{ox} \xrightarrow{h\nu} FAD^*_{ox} \xrightarrow{e^-} FADH^{\cdot *} \xrightarrow{e^-} FAD_{red}H_2.$$

After switch-off of the 470 nm excitation the FADH· absorption partly recovered (Fig. 11b) similar to the partial FAD_{ox} recovery seen in Figs. 8a and 9a.

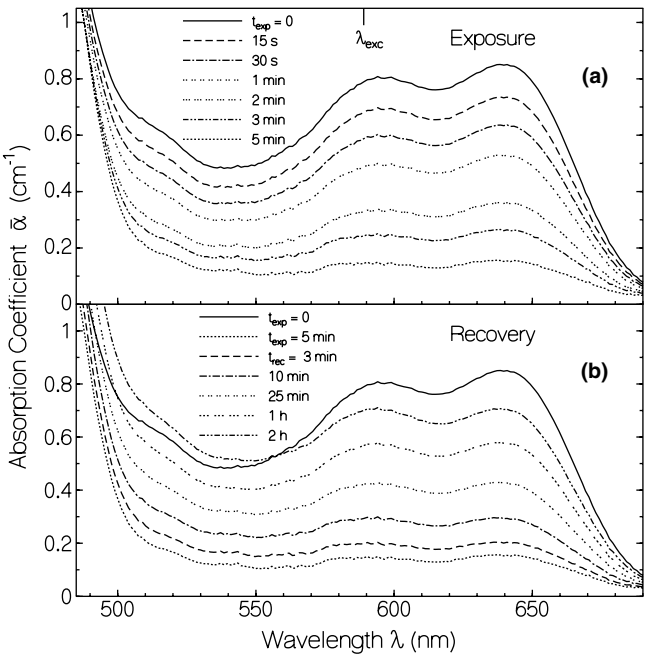

Fig. 10. Spectral photo-cycle behaviour of FADH· in cry3. (a) Absorption change due to excitation. Excitation wavelength, $\lambda_{exc} = 589$ nm; excitation intensity, $I_{exc} = 0.00254$ W cm^{-2}. The exposure times, t_{exp}, are given in the figure. (b) Absorption recovery in the dark after 5 min of exposure. The dark times, t_{rec}, are given in the figure.

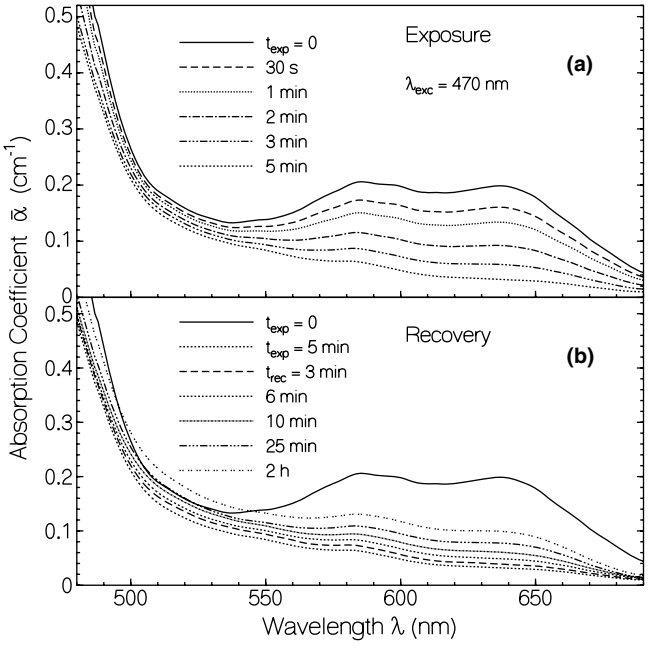

Fig. 11. Spectral photo-cycle behaviour of FAD_{ox} in absorption region of FADH· in cry3. (a) Absorption change due to excitation. Excitation wavelength, $\lambda_{exc} = 470$ nm; excitation intensity, $I_{exc} = 0.0105$ W cm^{-2}. The exposure times, t_{exp}, are given in the figure. (b) Absorption recovery in the dark after 5 min of exposure. The dark times, t_{rec} are given in the figure.

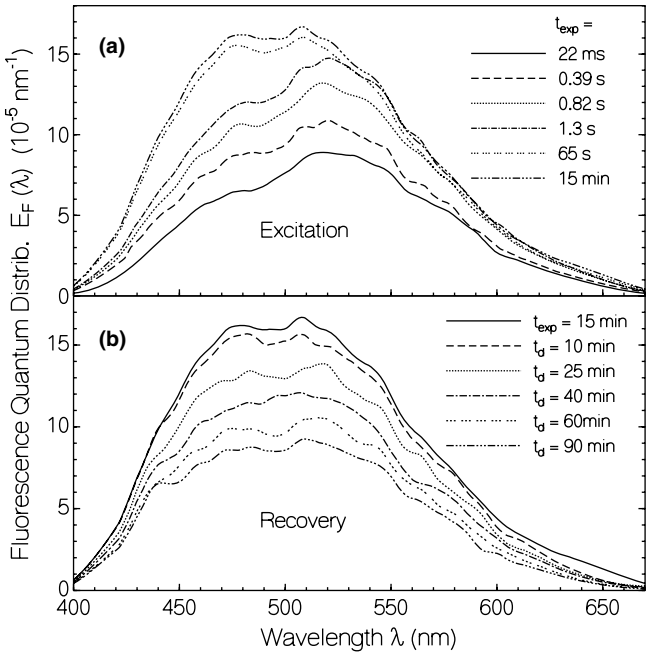

Fig. 12. Fluorescence quantum distribution of cry3 in pH 7.5 buffer at several times, t_{exp}, during light exposure at $\lambda_{exc} = 365$ nm with $I_{exc} = 4.5 \times 10^{-3}$ W cm^{-2} (a), and at several times, t_d, in the dark after light switch-off (b).

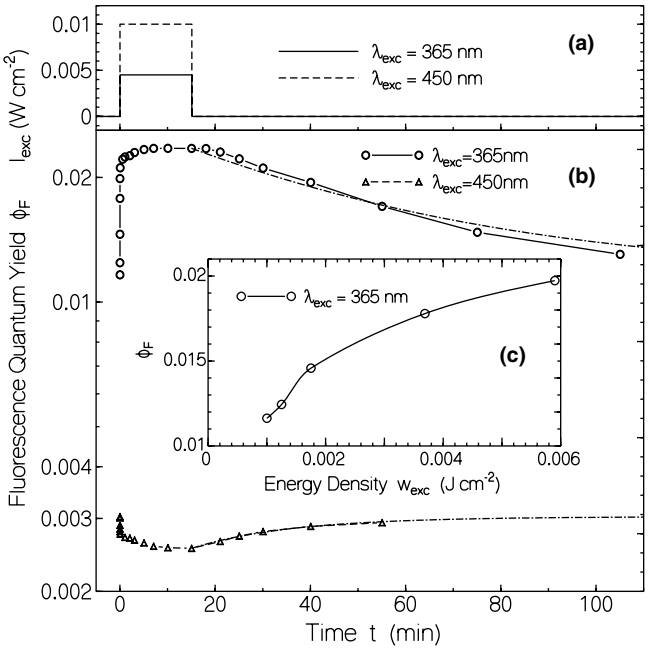

Fig. 13. Temporal development of fluorescence quantum yield, ϕ_F, during light exposure of 15 min and after light exposure (b). Light excitation profiles are given in (a). Single exponential recovery fits give $\tau_{F,rec}$-($\lambda_{exc} = 365$ nm) = 52 min and $\tau_{F,rec}(\lambda_{exc} = 450$ nm) = 23 min. Inset (c) shows fluorescence quantum yield as a function of exposed energy density (exposure time for each point 1 s, time separation between each experimental point 2 min).

The temporal development of the fluorescence quantum distributions of cry3 during light exposure ($\lambda_{exc} = 365$ nm, $I_{exc} = 4.5 \times 10^{-3}$ W cm^{-2}) and after light switch-off is shown in Fig. 12a and b, respectively. The distributions are shown for magic-angle fluorescence detection. The fluorescence signal quickly rises due to exposure and then levels off (putative signalling state formation). The fluorescence is dominated by MTHF emission. The rise in fluorescence is thought to be due to photo-induced protein conformation changes lowering the efficiency of charge transfer between excited MTHF and an interacting amino acid residue of the surrounding protein. It should be noticed that photo-induced electron transfer is strongly dependent on the distance between electron donor and electron acceptor [34]. At the beginning the FAD_{ox} fluorescence contribution around 520 nm is clearly seen. It is dominated by Förster-type energy transfer from MTHF to FAD_{ox}. At longer exposure times the FAD_{ox} fluorescence contribution reduces because of FAD_{ox} reduction to non-fluorescent $FAD_{red}H_2$.

In the dark the MTHF fluorescence relaxes to the dark-adapted situation of lower fluorescence quantum efficiency. In the back relaxation process the FAD_{ox} fluorescence is not fully recovered. This is thought to be partly due to some permanent $FAD_{red}H_2$ formation, and partly due to not complete re-structuring to the original protein structure.

In Fig. 13 the temporal development of the fluorescence quantum yield of cry3 in pH 7.5 buffer during light exposure and in the dark after light switch-off is shown. The light excitation profiles are shown in part (a), and the temporal fluorescence quantum yield development is shown in part (b). The situations are shown for excitation at $\lambda_{exc} = 365$ nm (data from Fig. 12) and at $\lambda_{exc} = 450$ nm. The fluorescence for $\lambda_{exc} = 365$ nm rises steeply a factor of two, and the fluorescence for $\lambda_{exc} = 450$ nm drops steeply a tiny amount due to putative signalling-state formation (protein re-conformation). The further slow decrease of fluorescence efficiency for $\lambda_{exc} = 450$ nm is caused by FAD_{ox} reduction. In the dark the fluorescence efficiencies recover back to the initial dark adapted situation. The time constants of single-exponential fluorescence recovery are $\tau_{F,rec}(365$ nm) ≈ 52 min and $\tau_{F,rec}(450$ nm) ≈ 23 min.

Bringing the cry3 sample to the putative signalling state by light excitation at $\lambda_{exc} = 470$ nm and probing the fluorescence emission at $\lambda_{F,pr} = 428$ nm by picosecond laser pulse excitation at 400 nm again gives a rise of the fluorescence signal by a factor of two compared to the dark-adapted situation. In this case the FAD_{ox} excitation is thought to increase the distance between the MTHF and amino acid charge transfer pair and thereby causes the increased MTHF fluorescence.

The dependence of the cry3 fluorescence quantum yield on the accumulated excitation energy density, w_{exc}, at $\lambda_{exc} = 365$ nm is shown in Fig. 13c (exposure time was short compared to recovery time of protein rearrangement). The excitation energy density, w_{sat}, where the rise in fluorescence quantum yield reaches half of its maximum value, is $w_{sat} \approx 4.2 \times 10^{-3}$ J cm^{-2}. The saturation energy density for the photo-induced MTHF fluorescence increase

is given by [35] $w_{sat} = hv_{exc}/(\sigma_{a,exc}\phi_{F,rise,MTHF})$, where $\sigma_{a,exc}$ is the absorption cross-section of cry3 at the excitation wavelength $\lambda_{exc} = c_0/v_{exc}$ (c_0 is speed of light in vacuum) and $\phi_{F,rise,MTHF}$ is the quantum efficiency of photo-induced charge transfer reduction. The experimental parameters of $\lambda_{exc} = 365$ nm, $\sigma_{a,exc} = 1.24 \times 10^{-16}$ cm^2, $w_{sat} \approx 4.2 \times 10^{-3}$ J cm^{-2} give $\phi_{F,rise,MTHF} \approx 1$. This result means that each absorbed photon in cry3 modifies the protein structure (larger distance between charge transfer partners). The slight reduction of the fluorescence quantum yield of FAD_{ox} seen in Fig. 13b occurs also with high efficiency ($\phi_{F,decrease,FAD} \approx 1$) (slightly nearer distance between charge transfer partners).

4. Discussion

4.1. Absorption spectra analysis

In photolyases [30,31,36–44] and cryptochromes [44,45], having MTHF as cofactor a spectral shift of the absorption of MTHF from 358 nm in aqueous solution to 383 nm in the protein is commonly observed. A protein–MTHF interaction is made responsible for this spectral shift. For *E. coli* DNA photolyase this was shown unambiguously by observing the spectral red shift in the photolyase protein without the presence of FAD [31]. In [30] evidence is given by site-directed mutagenesis studies, that a nearby glutamate residue plays an important role in the observed red-shift. For cryptochrome 1 VcCry1 from *Vibrio cholerae* [45] an absorption spectroscopic analysis showed that FAD is mainly present in the form of $FAD_{red}H^-$ and that the MTHF absorption is red-shifted.

Our absorption spectral analysis of cry3 presented in Fig. 2 indicates the presence of about 5% neutral FAD semiquinone ($FADH^{\cdot}$), approximately 40% neutral oxidized FAD (FAD_{ox}), and about 55% reduced FAD (either $FAD_{red}H_2$ or $FAD_{red}H^-$). The remaining absorption contribution is attributed to MTHF. Its shape agrees with the red-shifted absorption spectrum of MTHF in *E. coli* photolyase.

The absorption spectroscopic results of Figs. 6–9 indicate that for weak light exposure small MTHF and FAD_{ox} absorption changes occur probably due to reversible photo-induced slight protein re-structuring (quantum efficiencies $\phi_{a,rise,MTHF} \approx \phi_{a,rise,FAD} \approx 0.1$). At medium excitation intensities cry3 delivers a reversible photo-cycle behaviour with FAD photo-cycle ($FAD_{ox} - FAD_{red}H_2 - FAD_{ox}$, $\phi_{FAD,red} \approx 0.0018$) and MTHF photo-cycle (MTHF – MTHF′ – MTHF, $\phi'_{MTHF} \approx 2.9 \times 10^{-4}$). For prolonged high intensity excitation permanent absorption changes occur likely because of irreversible FAD reduction to $FAD_{red}H_2$ or $FAD_{red}H^-$ (protein stabilized, conversion of reversible $FAD_{red}H_2$ to irreversible $FAD_{red}H_2$ with $\phi_{FAD,red,per} \approx 4.3 \times 10^{-4}$), and MTHF conversion to MTHF″ probably caused by cofactor release followed by hydrolysis with $\phi_{MTHF''} \approx 3.7 \times 10^{-5}$. The identity of the formed MTHF products has to be determined in future experiments. Photo-excitation of $FADH^{\cdot}$ in cry3 causes an efficient reversible transfer to $FAD_{red}H_2$ or $FAD_{red}H^-$ ($\phi_{sq,red} \approx 0.07$).

4.2. Fluorescence analysis and discussion of Förster-type energy transfer

The fluorescence efficiency of free MTHF in aqueous solution at pH 2.5 ($\phi_F \approx 0.0025$) is rather low. The radiative lifetime of MTHF is determined from the S_0–S_1 absorption cross-section spectrum and the shape of the fluorescence quantum distribution by use of the Strickler-Berg formula [46–48]

$$\tau_{rad}^{-1} = \frac{8\pi c_0 n_F^3}{n_A} \frac{\int_{em} E_F(\lambda)\,d\lambda}{\int_{em} E_F(\lambda)\lambda^3\,d\lambda} \int_{abs} \frac{\sigma_a(\lambda)}{\lambda}\,d\lambda, \quad (5)$$

where c_0 is the vacuum light velocity, n_A and n_F are the average refractive indices in the S_0–S_1 absorption region (abs) and the S_1–S_0 emission region (em). A value of $\tau_{rad} = 7.6$ ns is obtained (upper border of absorption wavelength $\lambda_u = 303$ nm, $n_A = 1.3475$, $n_F = 1.337$). A fluorescence lifetime of $\tau_F \approx 36$ ps is estimated from the relation, $\tau_F = \phi_F\tau_{rad}$. Similar fluorescence lifetimes are reported in [31], but higher fluorescence quantum yields are given there.

The fluorescence quantum yield of dark-adapted cry3 in pH 7.5 buffer at $\lambda_{exc} = 450$ nm is $\phi_F \approx 0.003$. At $\lambda_{exc} = 365$ nm the dark-adapted fluorescence is $\phi_F \approx 0.012$ due to MTHF emission and FAD_{ox} emission caused by MTHF to FAD_{ox} energy transfer. In the light-adapted state the fluorescence quantum yield of MTHF in cry3 increases by about a factor of two because of modified surrounding protein conformation which reduces the fluorescence quenching by photo-induced charge transfer. The quantum efficiency of photo-induced fluorescence rise was found to be $\phi_{F,rise,MTHF} \approx 1$.

In two-chromophore-systems Förster-type energy transfer occurs from the short-wavelength absorbing component (donor, here: MTHF) to the long-wavelength absorbing component (acceptor, here: FAD_{ox}, $FAD_{red}H_2$, $FADH^{\cdot}$). In the following the quantum efficiencies of Förster-type energy transfer, ϕ_{ET}, between MTHF and FAD_{ox}, $FAD_{red}H_2$, and $FADH^{\cdot}$ are estimated. ϕ_{ET} is generally given by

$$\phi_{ET} = \frac{k_{ET}}{k_{tot}} = \frac{k_{ET}}{k_{ET} + k_{F,0,d}} = \frac{k_{ET}}{k_{ET} + (\phi_{F,0,d}\tau_{rad,d})^{-1}}, \quad (6)$$

where k_{ET} is the rate of energy transfer, k_{tot} is the total rate constant of the donor, and $k_{F,0,d} = \tau_{F,0,d}^{-1}$ is the rate of S_1–S_0 relaxation of the donor in the absence of energy transfer. $\phi_{F,0,d}$ is the fluorescence quantum yield of the donor in the absence of energy transfer (absence of acceptor), and $\tau_{rad,d}$ is the radiative lifetime of the donor. The rate of energy transfer is given by [49,50]

$$k_{ET} = k_{F,0,d}\left(\frac{R_0}{R_d}\right)^6 = k_{rad,d}\left(\frac{R'_0}{R_d}\right)^6, \quad (7)$$

where R_0 is the critical Förster distance where $k_{ET} = k_{F,0,d}$, R_0' is the critical Förster distance where $k_{ET} = k_{rad,d}$, and R_d is the distance between the energy transfer partners. The Förster distance, R_0', is given by the relation [49–51]

$$R_0'^6 = \frac{9\kappa^2}{128\pi^5 n^4} \int E_F'(\lambda)\sigma_a(\lambda)\lambda^4 \, d\lambda, \quad (8)$$

where n is the average refractive index in the overlap region of absorption and emission, $E_F'(\lambda) = E_F(\lambda)/\int E_F(\lambda') \, d\lambda' = E_F(\lambda)/\phi_F$ is the normalized fluorescence quantum distribution of the donor, and $\sigma_a(\lambda)$ is the absorption cross-section of the acceptor. The orientation factor κ is determined by the orientation of the transition dipole moments of the interacting molecules D (donor) and A (acceptor) according to [49]

$$\kappa = \cos(\varphi_{DA}) - 3\cos(\varphi_D)\cos(\varphi_A), \quad (9)$$

where φ_D and φ_A are the angles of the donor and acceptor transition dipole moments to the connection line between D and A, and φ_{DA} is the mutual angle between the transition dipole moments. Depending on the orientation of transition dipole moments it may vary between 0 and 2. For a statistical isotropic orientation of the transition dipole moments it is $\kappa^2 = 2/3$ [49].

For the considered situations of energy transfer from MTHF to FAD in cry3, the distance between donor and acceptor is $R_d = 1.5247$ nm, and the angles are $\varphi_D = 38.91°$, $\varphi_A = 69.44°$, and $\varphi_{DA} = 86.40°$ [52], giving $\kappa^2 = 0.573$. The calculated critical Förster distances are $R_0'(\text{MTHF–FAD}_{ox}) = 3.93$ nm, $R_0'(\text{MTHF–FAD}_{red}H_2) = 2.68$ nm, and $R_0'(\text{MTHF–FADH}^{\cdot}) = 3.84$. The energy transfer rates are calculated to be $k_{ET}(\text{MTHF} \rightarrow \text{FAD}_{red}H_2) \approx 4 \times 10^9 \text{ s}^{-1}$, $k_{ET}(\text{MTHF} \rightarrow \text{FAD}_{ox}) \approx 3.9 \times 10^{10} \text{ s}^{-1}$, and $k_{ET}(\text{MTHF} \rightarrow \text{FADH}^{\cdot}) \approx 3.6 \times 10^{10} \text{ s}^{-1}$ using $\tau_{rad} = 7.6$ ns. The quantum efficiencies of Förster-type energy transfer, ϕ_{ET} (Eq. (6)) cannot be determined accurately since the fluorescence quantum yield, $\phi_{F,0}$, of MTHF in cry3 in the absence of FAD is not known. Assuming as a lower limit $\phi_{F,0} = \phi_F \approx 0.012$ for dark-adapted cry3 and $\phi_{F,0} = \phi_F \approx 0.024$ for light-adapted cry3, we estimate as lower limits $\phi_{ET}(\text{MTHF–FAD}_{ox}$, dark-adapted) ≈ 0.78 and $\phi_{ET}(\text{MTHF–FAD}_{ox}$, light-adapted) ≈ 0.87.

The fluorescence lifetime measurements indicated the presence of at least two FAD_{ox} components with different fluorescence lifetime. One part with the fraction of 3.7% is thought to be due to non-correctly arranged FAD_{ox} in the binding pocket or free FAD_{ox} (long fluorescence lifetime). The main fraction of 96.3% is due to FAD_{ox} non-covalently fixed in the binding pocket of the protein in an U-shaped conformation (short fluorescence lifetime because of photo-induced reductive electron transfer from adenine to isollaoxazine moiety [26,53–58]). The fluorescence lifetime of the non-covalently bound FAD may also be shortened by photo-induced reductive electron transfer between any adjacent Trp, Tyr, Phe, His, or Cys amino-acid residue and the isoalloxazine moiety of FAD [59–62]. A detailed analysis of the amino acid residue arrangement from crystal structure studies would be necessary to find out the electron transfer pathways.

Ultrafast dynamics studies on the cryptochrome VcCry1 from *Vibrio cholerae* containing MTHF and FAD were well explained by resonance energy transfer from $MTHF^*$ to $FADH^-$, $MTHF^*$ to FAD_{ox}, and by $MTHF^*$ emission in protein free of FAD [45].

4.3. Photo-cycle dynamics

The spectroscopic analysis presented above revealed photo-cycles for protein conformation changes, FAD-semiquinone reduction, oxidized FAD reduction, and MTHF conversion. Additionally conversion of oxidable reduced FAD to permanent reduced FAD and permanent conversion of MTHF was observed. The photo-dynamics of cry3 is illustrated in the schemes (S1)–(S4).

$$\text{MTHF-Cry3}_{da}\text{-FAD}_{ox} \underset{\text{dark}}{\overset{h\nu,\phi_{protein}}{\rightleftharpoons}} \text{MTHF-Cry3}_{la}\text{-FAD}_{ox} \quad (S1)$$

Scheme S1 shows the cycle of the protein conformational change. The dark-adapted cry3, MTHF-$Cry3_{da}$-FAD, is modified to the light-adapted form, MTHF-$Cry3_{la}$-FAD with a high quantum efficiency of $\phi_{protein} \approx \phi_{F,rise,MTHF} \approx \phi_{F,decrease,FAD} \approx 1$. After light switch-off there occurs back-recovery to the dark form with rather slow recovery time of $\tau_{protein,rec} \approx 60$ min. Slight absorption changes on MTHF and FAD_{ox} were observed with a quantum efficiency of $\phi_{a,rise,MTHF} \approx \phi_{a,rise,FAD} \approx 0.1$.

$$\text{MTHF-Cry3-FADH}^{\cdot} \underset{\text{dark}}{\overset{h\nu,\phi_{sq,red}}{\rightleftharpoons}} \text{MTHF-Cry3}'\text{-FAD}_{red}H_2 \quad (S2)$$

Scheme S2 shows the photo-cycle dynamics of FAD-semiquinone reduction. MTHF-Cry3-$FADH^{\cdot}$ is transferred to MTHF-$Cry3'$-$FAD_{red}H_2$ by photo-excitation. The apoprotein Cry3 changes its structure to $Cry3'$ because of electron transfer to $FADH^{\cdot}$. The FAD-semiquinone reduction is rather efficient. A quantum yield of $\phi_{sq,red} \approx 0.07$ was determined. A recovery to $FADH^{\cdot}$ in the dark was observed with a time constant of $\tau_{sq,rec} \approx 60$ min.

$$\begin{array}{l} \text{MTHF-Cry3-FAD}_{ox} \underset{\text{dark}}{\overset{h\nu,\ \phi_{FAD,red}}{\rightleftharpoons}} \text{MTHF-Cry3''-FAD}_{red}H_2 \\ \qquad\qquad\qquad\qquad\qquad\qquad \Big\downarrow \ h\nu,\ \phi_{FAD,red,per} \\ \qquad\qquad\qquad\qquad\qquad\qquad \text{MTHF-Cry3''-FAD}_{red}H_{2,per} \end{array} \quad (S3)$$

Scheme S3 displays the photo-cycle dynamics of FAD_{ox} reduction, and of permanent $FAD_{red}H_2$ formation from reversible $FAD_{red}H_2$. MTHF-Cry3-FAD_{ox} is photo-converted to MTHF-$Cry3''$-$FAD_{red}H_2$ with a low quantum efficiency of $\phi_{FAD,red} \approx 0.0018$. The back re-oxidation is slow; a recovery time of $\tau_{rec} \approx 50$ min was measured. Prolonged excitation converts the re-oxidable $FAD_{red}H_2$ in

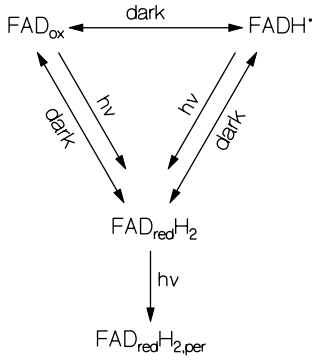

Fig. 14. FAD state composition in cry3 (for details see text).

cry3 to non-oxidable $FAD_{red}H_{2,per}$. Possibly some unique protein conformation change is responsible for this behaviour. The quantum efficiency of conversion to permanent reduced FAD was found to be $\phi_{FAD,red,per} \approx 4 \times 10^{-4}$.

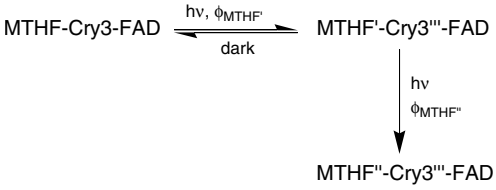

(S4)

The photo-cycle dynamics of conversion of MTHF-Cry3-FAD to MTHF′-Cry3‴-FAD and back-recovery is shown in scheme S4. A conversion quantum efficiency of $\phi_{MTHF'} \approx 2.9 \times 10^{-4}$ was determined. The back-recovery time in the dark was $\tau_{MTHF,rec} \approx 30$ min. Prolonged light exposure caused irreversible MTHF conversion to MTHF″ with a quantum efficiency of $\phi_{MTHF''} \approx 3.7 \times 10^{-5}$.

A reaction and equilibration scheme for FAD in cry3 is displayed in Fig. 14. In the dark there is an equilibrium between FAD_{ox}, FADH$^{\bullet}$, and $FAD_{red}H_2$. Photo-excitation reduces FAD_{ox} and FADH$^{\bullet}$ to $FAD_{red}H_2$. Prolonged light exposure modifies re-oxidable $FAD_{red}H_2$ to non-oxidable $FAD_{red}H_{2,per}$.

Recently the photo-cycle behaviour of cry1 from *Arabidopis thaliana* was studied in vitro by Fourier transform infrared (FTIR) and UV/VIS difference spectroscopy [63]. There, in the dark state the cofactor FAD is present in oxidized form (FAD_{ox}), and photo-excitation transfers FAD_{ox} to FADH$^{\bullet}$ which slowly recovers back to FAD_{ox} in the dark. No presence and involvement of MTHF in the in vivo cry1 photo-cycle dynamics was observed. These studies clearly show the different cofactor compositions of dark-adapted cry1 and cry3 and the different photo-biological dynamics of cry1 and cry3 caused by blue-light exposure.

5. Conclusions

The photodynamic behaviour of the cofactors FAD and MTHF in cryptochrome 3 from the plant *Arabidopsis thaliana* has been studied in vitro. A population-equilibrium between FAD_{ox}, FADH$^{\bullet}$, and $FAD_{red}H_2$ (or $FAD_{red}H^-$) exists in the dark. Depending on the excitation intensity and the excitation wavelength different photo-cycles are acting. Reversible protein conformation changes occur with high quantum efficiency requiring only weak light exposure. FAD-semiquinone is reversibly converted to reduced FAD with rather high efficiency. The photo-cycle of FAD_{ox} reduction to fully reduced FAD and dark recovery as well as the photo-cycle of MTHF conversion to MTHF′ and dark recovery have only moderate quantum efficiencies. Prolonged intense light exposure causes permanent FAD reduction and MTHF″ formation.

Fluorescence lifetime measurements revealed the presence of a small fraction (≈1.5%) of FAD_{ox} molecules not properly fixed in the cry3 binding pocket (long fluorescence lifetime). The short fluorescence lifetime of FAD_{ox}, which is non-covalently bound to the apoprotein, is in agreement with U-shaped arrangement between the isoalloxazine moiety and the adenine moiety of FAD. Also reductive electron transfer from adjacent amino-acids like Trp, Tyr, Phe, His, or Cys to FAD are thought to contribute to the fluorescence lifetime shortening [59–62].

Future crystal structure analysis may give additional mechanistic insight into the acting photo-cycle processes. Physiological studies with cry3 RNAi-, T-DNA-tagged and overexpressing lines are underway to reveal the biological function of cry3.

Acknowledgements

The authors are very grateful to Mr. P. Zirak and Mr. A.K. Bansal for experimental help. They thank A. Merkel for mechanical assistance. We acknowledge DFG grant support to the Research Group FOR 526 "Sensory Blue Light Receptors" (Grant BA 985/10-1 to A.B., Pe217/33-1 to A.P., and Di299/7-1 to B.D.) which enabled this collaborative work.

References

[1] R. Briggs, J.L. Spudich (Eds.), Handbook of Photosensory Receptors, Wiley–VCH Verlag, Weinheim, Germany, 2005.
[2] A. Batschauer (Ed.), Photoreceptors and Light Signalling, Comprehensive Series in Photochemical & Photobiological Sciences, The Royal Society of Chemistry, Cambridge, UK, 2003.
[3] A. Sancar, Structure and function of DNA photolyase and cryptochrome blue-light photoreceptors, Chem. Rev. 103 (2003) 2203–2238.
[4] A. Sancar, Cryptochrome: The second photoactive pigment in the eye and its role in circadian photoreception, Annu. Rev. Biochem. 69 (2000) 31–67.
[5] C. Lin, D. Shalitin, Cryptochrome structure and signal transduction, Annu. Rev. Plant Biol. 54 (2003) 469–496.
[6] M. Gomelsky, G. Klug, BLUF: a novel FAD-binding domain involved in sensory transduction in microorganisms, Trends Biochem. Sci. 27 (2002) 497–500.
[7] S. Masuda, C.E. Bauer, AppA is a blue light photoreceptor that antirepresses photosynthesis gene expression in *Rhodobacter sphaeroides*, Cell 110 (2002) 613–623.
[8] M. Iseki, S. Matsunaga, A. Murakami, K. Ohno, K. Shiga, K. Yoshida, M. Sugai, T. Takahashi, T. Hori, M. Watanabe, A blue-light-activated adenylyl cyclase mediates photoavoidance in *Euglena gracilis*, Nature 415 (2002) 1047–1051.

[9] K. Okajima, S. Yosihara, J. Fukushima, X. Geng, M. Katayama, S. Higashi, M. Watanabe, S. Sato, S. Tabata, Y. Shibata, S. Itoh, M. Ikeuchi, Biochemical and functional characterization of BLUF-type flavin-binding proteins of two species of cyanobacteria, J. Biochem. (Tokyo) 137 (2005) 741–750.
[10] S. Masuda, K. Hasegawa, A. Ishii, T. Ono, Light-induced structural changes in a putative blue-light receptor with a novel FAD binding fold sensor of blue-light using FAD (BLUF); Slr1694 of *Synechocystis* sp. PCC6803, Biochemistry 43 (2004) 5304–5313.
[11] A. Jung, T. Domratcheva, M. Tarutina, Q. Wu, W. Ko, R.L. Shoeman, M. Gomelsky, K.H. Gardner, I. Schlichting, Structure of a bacterial BLUF photoreceptor: insights into blue light-mediated signal transduction, PNAS 102 (2005) 12350–12355.
[12] P. Zirak, A. Penzkofer, T. Schiereis, P. Hegemann, A. Jung, I. Schlichting, Photodynamics of the small BLUF protein BlrB from *Rhodobacter sphaeroides*, J. Photochem. Photobiol. B: Biol. 180 (2006) 180–196.
[13] W.R. Briggs, J.M. Christie, Phototropins 1 and 2: versatile plant blue-light receptors, Trends Plant Sci. 7 (2002) 204–210.
[14] K. Malhotra, S.-T. Kim, A. Batschauer, L. Dawut, A. Sancar, Putative blue-light photoreceptors from *Arabidopsis thaliana* and *Sinapis alba* with a high degree of sequence homology to DNA photolyase contain the two photolyase cofactors but lack DNA repair activity, Biochemistry 34 (1995) 6892–6899.
[15] C. Lin, D.E. Robertson, M. Ahmad, A.A. Raibekas, M.S. Jorns, P.L. Dutton, A.R. Cashmore, Association of flavin adenine dinucleotide with the *Arabidopsis* blue light receptor CRY1, Science 269 (1995) 968–970.
[16] M. Ahmad, A.R. Cashmore, Hy4 gene of *A. thaliana* encodes a protein with characteristics of blue-light photoreceptor, Nature 366 (1993) 162–166.
[17] P.D. Hoffman, A. Batschauer, J.B. Hays, AT-PHH1, a novel gene from *Arabidopsis thaliana* related to microbial photolyases and plant blue light photoreceptors, Mol. Gen. Genet. 253 (1996) 259–265.
[18] T. Kleine, P. Lockhart, A. Batschauer, An *Arabidopsis* protein closely related to *Synechocystis* cryptochrome is targeted to organelles, Plant J. 35 (2003) 93–103.
[19] R. Brudler, K. Hitomi, H. Daiyasu, H. Toh, K. Kucho, M. Ishiura, M. Kanehisa, V.A. Roberts, T. Todo, A. Trainer, E.D. Getzoff, Identification of a new cryptochrome class: structure, function, and evolution, Mol. Cell 11 (2003) 59–67.
[20] C. Lin, Blue light receptors and signal transduction, Plant Cell 14 (Suppl.) (2002) S207–S225.
[21] H. Guo, H. Yang, T.C. Mockler, C. Lin, Regulation of flowering time by *Arabidopsis* photoreceptors, Science 279 (1998) 1360–1363.
[22] R. Pokorny, T. Klar, L.-O. Essen, A. Batschauer, Crystallization and preliminary X-ray analysis of cryptochrome 3 from *Arabidopsis thaliana*, Acta Crystallogr. F 61 (2005) 935–938.
[23] A. Penzkofer, W. Leupacher, Fluorescence behaviour of highly concentrated rhodamine 6G solutions, J. Luminesc. 37 (1987) 61–72.
[24] W. Holzer, M. Pichlmaier, A. Penzkofer, D.D.C. Bradley, W.J. Blau, Fluorescence spectroscopic behaviour of neat and blended conjugated polymer thin films, Chem. Phys. 246 (1999) 445–462.
[25] W.H. Melhuish, Quantum efficiencies of fluorescence of organic substances: effect of solvent and concentration of the fluorescent solute, J. Phys. Chem. 65 (1961) 229–235.
[26] S.D.M. Islam, T. Susdorf, A. Penzkofer, P. Hegemann, Fluorescence quenching of flavin adenine dinucleotide in aqueous solution by pH dependent isomerisation and photo-induced electron transfer, Chem. Phys. 295 (2003) 137–149.
[27] F. Müller (Ed.), Chemistry and Biochemistry of Flavoenzymes, vol. 1, CRC Press, Boca Raton, FL, 1991.
[28] B.A. Palfey, V. Massey, Flavin-dependent enzymes, in: M. Sinnott (Ed.), Comprehensive Biological Catalysis. A Mechanistic Reference, Radical Reactions and Oxidation/Reduction, vol. III, Academic Press, San Diego, USA, 1997, pp. 83–154.
[29] J.L. Johnson, S. Hamm-Alvarez, G. Payne, G.B. Sancar, K.V. Rajagopalan, A. Sancar, Identification of the second chromophore of *Escherichia coli* and yeast DNA photolyases as 5,10-methenyltetrahydrofolate, Proc. Natl. Acad. Sci. USA 85 (1988) 2046–2050.
[30] A.A. Henry, R. Jimenez, D. Hanway, F.E. Romesberg, Preliminary characterization of light harvesting in *E. coli* DNA photolyase, ChemBioChem. 5 (2004) 1088–1094.
[31] S.-T. Kim, P.F. Heelis, T. Okamura, Y. Hirata, N. Magata, A. Sancar, Determination of rates and yields of interchromophore (folate → flavin) energy transfer and intermolecular (flavin → DNA) electron transfer in *Escherichia coli* photolyase by time-resolved fluorescence and absorption spectroscopy, Biochemistry 30 (1991) 11262–11270.
[32] P. Drössler, W. Holzer, A. Penzkofer, P. Hegemann, pH dependence of the absorption and emission behaviour of riboflavin in aqueous solution, Chem. Phys. 282 (2002) 429–439.
[33] J.E. Baggott, Hydrolysis of 5,10-methenyltetrahydrofolate to 5-formyltetrahydrofolate at pH 2.5 to 4.5, Biochemistry 39 (2000) 14647–14653.
[34] M. Orrit, The Motions of an Enzyme Soloist, Science 302 (2003) 239–240.
[35] M. Hercher, An analysis of saturable absorbers, Appl. Opt. 6 (1967) 947–953.
[36] G. Payne, P.F. Heelis, B.R. Rohrs, A. Sancar, The active form of *Escherichia coli* DNA photolyase contains a fully reduced flavin and not a flavin radical, both in vivo and in vitro, Biochemistry 26 (1987) 7121–7127.
[37] S.T. Kim, P.F. Heelis, A. Sancar, Energy transfer (deazaflavin → $FADH_2$) and electron transfer ($FADH_2$ → T⟨⟩T) kinetics in *Anacystis nidulans* photolyase, Biochemistry 31 (1992) 11244–11248.
[38] P.F. Heelis, G. Payne, A. Sancar, Photochemical properties of *Escherichia coli* DNA photolyase: selective photodecomposition of the second chromophore, Biochemistry 26 (1987) 4634–4640.
[39] M.S. Jorns, G.B. Sancar, A. Sancar, Identification of a neutral flavin radical and characterization of a second chromophore in *Escherichia coli* DNA photolyase, Biochemistry 23 (1984) 2673–2679.
[40] H. Wang, C. Saxena, D. Quan, A. Sancar, D. Zhong, Femtosecond dynamics of flavin cofactor in DNA photolyase: radical reduction, local solvation, and charge recombination, J. Phys. Chem. B 109 (2005) 1329–1333.
[41] C. Saxena, A. Sancar, D. Zhong, Femtosecond dynamics of DNA photolyase: energy transfer of antenna initiation and electron transfer of cofactor reduction, J. Phys. Chem. B 108 (2004) 18026–18033.
[42] B. Wang, M.S. Jorns, Reconstitution of *Escherichia coli* DNA photolyase with various folate derivatives, Biochemistry 28 (1989) 1148–1152.
[43] M.S. Jorns, B. Wang, S.P. Jordan, L.P. Chanderkar, Chromophore function and interaction in *Escherichia coli* DNA photolyase: reconstitution of the apoenzyme with pterin and/or flavin derivatives, Biochemistry 29 (1990) 552–561.
[44] E.N. Worthingon, I.H. Kavakli, G. Berrocal-Tito, B.E. Bondo, A. Sancar, Purification and characterization of three members of the photolyase/cryptochrome family blue-light photoreceptors from *Vibrio cholerae*, J. Biol. Chem. 278 (2003) 39143–39154.
[45] C. Saxena, H. Wang, I.H. Kavakli, A. Sancar, D. Zhong, Ultrafast dynamics of resonance energy transfer in cryptochrome, J. Am. Chem. Soc. 127 (2005) 7984–7985.
[46] S.J. Strickler, R.A. Berg, Relationship between absorption intensity and fluorescence lifetime of molecules, J. Chem. Phys. 37 (1962) 814–822.
[47] J.B. Birks, D.J. Dyson, The relations between the fluorescence and absorption properties of organic molecules, Proc. Roy. Soc. London, Ser. A 275 (1993) 135–148.
[48] A.V. Deshpande, A. Beidoun, A. Penzkofer, G. Wagenblast, Absorption and emission spectroscopic investigation of cyanovinyl-diethylaniline dye vapors, Chem. Phys. 142 (1990) 123–131.
[49] Th. Förster, Fluoreszenz organischer Verbindungen, Vandenhoeck and Ruprecht, Göttingen, 1951.
[50] G.R. Fleming, Chemical Applications of Ultrafast Spectroscopy, Oxford University Press, New York, 1986.

[51] F. Ammer, A. Penzkofer, P. Weidner, Concentration dependent fluorescence behaviour of Oxazine 750 and Rhodamine 6G in porous silicate xerogel monoliths, Chem. Phys. 192 (1995) 325–331.
[52] T. Klar, R. Pokorny, A. Batschauer, L.O. Essen (in preparation).
[53] J.R. Barrio, G.L. Tolman, N.J. Leonard, R.D. Spencer, G. Weber, Flavin 1,N^6-etheneadenine dinucleotide dynamic and static quenching of fluorescence, Proc. Natl. Acad. Sci. USA 70 (1973) 941–943.
[54] R.D. Spencer, G. Weber, Thermodynamics and kinetics of the intramolecular complex in flavin-adenine dinucleotide, in: Å. Åkeson, A. Ehrenberg (Eds.), Structure and Function of Oxidation Reduction Enzymes, Pergamon Press, Oxford, 1972, pp. 393–399.
[55] P.A.W. van den Berg, J. Widengren, M.A. Hink, R. Rigler, A.J.W.G. Visser, Fluorescence correlation spectroscopy of flavins and flavoenzymes: Photochemical and photophysical aspects, Spectrochim. Acta A 57 (2001) 2135–2144.
[56] A.J.W.G. Visser, Kinetics of stacking interactions in flavin adenine dinucleotide from time-resolved flavin fluorescence, Photochem. Photobiol. 40 (1984) 703–706.
[57] Ph. Wahl, J.C. Auchet, A.J.W.G. Visser, F. Müller, Time resolved fluorescence of flavin adenine dinucleotide, FEBS Lett. 44 (1974) 67–70.
[58] P.A.W. van den Berg, K.A. Feenstra, A.E. Mark, H.J.C. Berendsen, A.J.W.G. Visser, Dynamic conformations of flavin adenine dinucleotide: simulated molecular dynamics of the flavin cofactor related to the time-resolved fluorescence characteristics, J. Phys. Chem. B 106 (2002) 8858–8869.
[59] D. Zhong, A.H. Zewail, Femtosecond dynamics of flavoproteins: charge separation and recombination in riboflavine (vitamin B_2)-binding protein and in glucose oxidase enzyme, PNAS 98 (2001) 11867–11872.
[60] N. Mataga, H. Chosrowjan, Y. Shibata, F. Tanaka, Y. Nishina, K. Shiga, Dynamics and mechanisms of ultrafast fluorescence quenching reactions of flavin chromophores in protein nanospace, J. Phys. Chem. B 104 (2001) 10667–10677.
[61] P.A.W. van den Berg, A.J.W.C. Visser, Tracking molecular dynamics of flavoproteins with time-resolved fluorescence spectroscopy, in: B. Valeur, J.-C. Brochon (Eds.), New Trends in Fluorescence Spectroscopy: Applications to Chemical and Life Sciences, Springer-Verlag, New York, 2001, pp. 457–485.
[62] C.W.M. Kay, E. Schleicher, A. Kuppig, H. Hofner, W. Rüdiger, M. Schleicher, M. Fischer, A. Bacher, S. Weber, G. Richter, Blue light perception in plants. Detection and characterization of a light-induced neutral flavin radical in a C450A mutant of phototropin, J. Biol. Chem. 278 (2003) 10973–10982.
[63] T. Kottke, A. Batschauer, M. Ahmad, J. Heberle, Blue-light-induced changes in *Arabidopsis* cryptochrome 1 probed by FTIR difference spectroscopy, Biochemistry 45 (2006) 2472–2479.